University of Cape-Coast, Ghana

Faculty of Science

Department of Physics

The Third International Workshop on The Physics & Modern Applications of Lasers

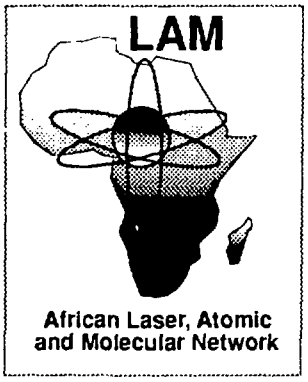

8th - 20th August, 1994

CONTENTS

NATIONAL ORGANISING COMMITTEE

1. Prof. S.K. Adjepong, Local Director, Laser Conference, UCC.
2. Prof A.N. deHeer-Amissah, Chairman, NOC, UCC., Cape-Coast.
3. Prof. C. Ameyaw-Akumfi, UCC, Cape-Coast.
4. Prof. J.K.A. Amuzu, Dept. of Physics, Univ. of Ghana, Legon.
5. Prof. F.K.A. Allotey, Chairman, GAEC, Kwabenya, Accra
6. Dr. (Mrs.) Aba Andam, Univ. of Science & Technology Kumasi
7. Dr Haruna Yakubu, UCC, Cape-Coast
8. Dr. S.Y. Mensah, UCC, Cape-Coast
9. Dr. V.P.Y. Gadzekpo, UCC, Cape-Coast
10. Dr. N.K. Asare-Boamah, UCC, Cape-Coast
11. Dr. P.K. Buah-Bassuah, Local Organiser, UCC Cape-Coast
12. Mr. P.K. Mensah, UCC, Cape-Coast

SUB-COMMITTEE

TECHNICAL

1.	DR. P.K. Buah-Bassuah	-	Convener
2.	Prof. A.N. deHeer-Amissah	-	Editor
3.	Dr. V.P.Y. Gadzekpo	-	Editor
4.	Dr. S.Y. Mensah		
5.	Dr. Kwakye		
6.	Dr. Haruna Yakubu		
7.	Dr. Eric Quaye		
8.	Dr. (Mrs.) Aba Andam		

CO-OPTED MEMBERS

1. Mr. G.K. Quainoo
2. Mr. Joojo Eghan
3. Mr. E.A. Johnson
4. Mr. Owusu Korkor
5. Mr. Rex Okoto

MANCIPLES COMMITTEE

1.	Dr. N.K. Asare-Boamah	-	Governor
2.	Prof. J.K.A. Amuzu	-	Member
3.	Dr. A.A. Addo-Quaye	-	Member
4.	Dr. John Blay Jnr.	-	Member
5.	Mr. P.K. Mensah	-	Member
6.	Mr. E. Quagraine	-	Member
7.	Mrs. Irene Annor-Frimpong	-	Member

PUBLICITY COMMITTEE

1.	Prof. A.N. deHeer-Amissah	-	Convener
2.	Prof. J.K.A. Amuzu	-	Member
3.	Prof. F.K.A. Allotey	-	Member
4.	Prof. S.K. Adjepong	-	Member
5.	Prof. C. Ameyaw-Akumfi	-	Member
6.	Dr. (Mrs.) Aba Andam	-	Member

LIST OF PARTICIPANTS

COUNTRY	NO. OF PARTICIPANTS
Algeria	2
Burundi	1
Congo	1
Cote D'Ivoire	2
Egypt	3
Ethiopia	2
Kenya	3
Mali	1
Morocco	2
Niger	1
Nigeria	6
Senegal	4
Sierra Leone	2
Sudan	2
Uganda	1
Zambia	1
Zaire	1
Zimbabwe	3
Botswana	1
Ghana (other part)	20
Ghana (Cape-Coast)	7

LIST OF LECTURERS

COUNTRY	SPEAKERS
U.K.	2
U.S.A.	3
Italy	2
France	1
Germany	1
Sweden	1

LIST OF LECTURERS - U.K

1. Prof J.C. Dainty
   Imperial College of Science
   Technology & Medicine
   Optics Sec., The Blackett Lab.,
   Prince Consort Board
   London SW7 2BZ

2. Dr. Jonathan Maxwell
   Imperial College of Science
   Technology & Medicine
   Opt. Sec., The Blackett Lab.,
   Prince Consort Board
   London SW7 2BZ

U.S.A.

1. Prof. Herbert Winful,
   Dept. of Elect. Engineering &
   Computer Science
   University of Michigan
   1301 Beal Avenue
   Ann Arbor, Michigan
   48109-2122

2. Prof. E. Kannatey-Asibu
   Dept of Mech. Engineering
   & Applied Mechanics
   University of Michigan
   2250 G.G. Brown
   Ann Arbor, Michigan
   48109-2125

3. Prof. Charles Brown
   Transmission Media Laboratory
   AT&T Bell Laboratories
   200 Northeast Express Way
   Norcross, Georgia

ITALY

1. Prof. G. Denardo
   The Head, Office of Ext. Activities
   Box 586, Miramare, 1-34100,
   Trieste, Italy

2. Dr. Riccardo Meucci
   Istituto Nazionale di Ottica
   Largo Enrico Fermi 6
   50125, Arcetri
   Firenze

FRANCE

1. Dr. Jean-Francois Lagargasson
   Hopital Lariboisiere
   Service de Biophysique
   Department Vision,
   10 avenue de verdum
   750110 Paris

LIST OF PARTICIPANTS

ALGERIA

1. Prof. Mokhtar Kemal Inal
   Institut des Sc. Exactes
   Department de physique
   BP 119, 1300 TLemcem

2. Dr. Taieb Gasmi
   Laboratoire des Laser
   & Application/CDTA
   BP 245 El Madania

BURUNDI

1. Dr. Pierre Nzohabonayo
   University of Burundi
   BP 1550 Bujumbura

CONGO

1. Mr. Paul-Sand Moussounda
   University Marien Ngouabi
   Faculte des Sciences
   Dept. de physique
   BP 69 Brazzaveile

COTE D'IVOIRE

1. Dr. S. Kedro Diomande
   University d' Abidjan
   Dept. de Physique
   22 BP 582, Abidjan

2. Dr. Rita C.A. Kakou
   University d' Abidjan
   Dept. de physique
   22 BP 582, Abidjan 22 RCI

SENEGAL

1. Prof. Ahmadou Wague
   Dept.. of Physics
   Faculty of Science & Tech.
   University of Cheikh Anta Diop
   Dakar

2. Dr. Serigne M. Gueye
   Faculte de Medicine
   et Pharmacie
   Univ. Cheikh Anta Diop
   Dakar

3. Dr. G.N. Thon
   Ecole Nacionale des
   Telecommunication
   Dakar

4. Dr. Ndeye Faye
   Dept. de physique
   Univ. Cheikh Anta Diop
   Dakar

SIERRA LEONE

1. Dr. George C. Ishiekwene
   C/o Mrs. Florence Charley
   Chief Police Officer
   Police Headquarters
   Freetown

2. Mr. Pascal Obed Egbenda
   Fourah Bay College
   Dept. of Chemistry
   Freetown

SUDAN

1. Mr. Ali Abubakar Abdalla
   Dept. of Physics
   Faculty of Science
   University of Khartoum
   Khartoum

2. Prof. Ali E. Sharaf El-Din
   Dept of Physics
   University of Khartoum
   Khartoum

UGANDA

1. Mr. Tom Otiti
   Dept. of Physics
   Makerere University
   P.O. Box. 7062 Kampala

MALI

1. Dr. Bakary Cisse
   General Secretary
   The Medical School of Bamako
   Bamako

ETHIOPIA

1. Dr. Fasseha Kassahun
   Dept. of Physics
   Addis Ababa University
   P. O. Box. 1176
   Addis Ababa

2. Mr. Takale Seda
   Dept. of Physics
   Addis Ababa University
   P. O. Box. 1176
   Addis Ababa

EGYPT

1. Dr. K.M.A. Kassem
   Mech. Power & Energy Dept.
   Fac. of Eng. & Techn.,
   Minia Univ. Minia

2. Mr. Taha El-Hosary
   Egyptian Meteo. Auth
   P.O. Box. 11784
   Koubry El Qubba

3. Dr. Sherif M. Khalil
   Plasma Physics & Nuclear Fussion Dept.
   Nuclear Research Centre
   Atomic Energy Authority, Cairo

KENYA

1. Miss Dorothy Odhiamabo
   Dept. of Telecomm. Eng.
   College of Telecomm. Techn
   P. O. Box. 30305, Nairobi

2. Dr. Dickson Oming'o
   Dept. of Telecom. Eng.
   Col. of Telecon. Tech.
   Box. 30303, Nairobi

3. Mr. Zakayo Mbugua
   Dept. of Physics
   Moi University
   P.O. Box. 1125, Eldoret

ZAMBIA

1. Dr. Shyam Singh
   Dept. of Zambia
   P. O. Box. 32379

   Lusaka

ZAIRE

1. Prof. Marambo Karem ena
   Institut Superieur
   Pedagolique de
   Lubambashi
   BP 1796, Lubambas

MOROCCO

1. Prof. Abedelfettah Barhadadi
   Ecole Normale Superire de Takaddoum
   Lab. de Physique des Semiconductors
   et de l'Energie Solaire
   BP 5M8, 1000 Rabat

ZIMBABWE

1. Dr. A.V. Gholap
   Dept. of Physics
   Univ. of Zimbabwe
   Mount Pleasant Box MP 167
   Harare

2 Dr. Sydney M. Chagwedera
   Dept. of Sc. & Maths Educ.
   Univ. of Zimbabwe
   Mount Pleasant Box MP 167
   Harare

3. Mr. C. Chiteme
   University of Zimbabwe
   Mount Pleasant
   Box. MP 167, Harare

NIGER

Mr. Mamadou A. Diallo
Agrhymet Regional Centre
BP 11011, Niamey

NIGERIA

1. Dr. M.S. Ababakar
College of Sci. & Technology
PMB 2021, Kaduna

2. Dr. M.A.C. Chendo
Dept. of Physics
University of Lagos
Akoka, Lagos

3. Dr. Gabriel Anene
Nnamdi Azikiwe University
Faculty of Natural Science
Dept. of Industrial Physics
PMB 5025, Awka,
Anambra State, Nigeria

4. Dr. G.O. Agyai
Dept. of Elec. & Eng. Sc.
Obafemi Awolowo Univ.
Ile-Ife, Nigeria

5. Dr. Esther O. Ugogi
Dept of Biological Sc.
University of Lagos
Anka-Yaba, Nigeria

6. Mr. David A. Ajadi
Dept. of Physics
College of Education
P.M.B. Ilorin
Kwara State, Nigeria.

7. Dr. M. Ugwa Onuu
Dept of Physics
University of Calabar
PMB 1115, Calabar
Cross River State, Nigeria

BOTSWANA

Dr. John Akintayo Adedoyin
Dept. of Physics
University of Botswana
Private Bag 0022
Gaborone, Botswana

FROM THE LOCAL CORDINATOR'S DESK

The Workshop, which is third of its kind as an activity of the office of External Activities of International Centre for Theoretical Physics, aims at exposing the participants to current activities and future prospects of Optical Physics in both pure and applied research as well as in development projects. Each subject will begin with an introduction and gradually proceed towards advanced topics for solving problems relevant to research and development. Afternoon sessions will be devoted to discussions and seminars.

The Workshop would exhibit some basic experimental set-up with the view to exposing students of high schools of science, technology, mathematics (STMC) to the practicality of the use of Lasers on the Continent.

SCOPE OF THE WORKSHOP

The main topics to be treated include:

- Basic in lasers, geometrical, physical and quantum optics
- Optical techniques for research, education and development in Africa;
- Application of Lasers in Optical Fibre Communication, Environmental Studies, Biomedicine, Chemistry, Agriculture, Engineering, Industry.

The Workshop aims at promoting closer links in optics and lasers among scientific institutions, industries and the African LAM Network by:

- Providing a forum for enhancing exchange of ideas among African scientists and scientists from other parts of the world;

- Encouraging International Commission for Optics (ICO), as well as other international Scientific organisations, to assist in the development and training of young scientists in optical and laser science.

A round table discussion on laser and optics for development will be organised.

The general outlook of our programmes conform with the activities of the African Laser Atomic and Molecular Network. The workshop aims

at encouraging African Scientists to project their work in Lasers which is composed of areas such as

AREA	NO. OF PAPERS
Environment	5
Metrology	10
Lasers	7
Optical Spectroscopy	5
Fibre Optics	2
Medicine	1
Chemistry	1
	31

A total of 31 papers on Lasers and optical fibres to be presented at this workshop are of much relevance to our national development.

We are most grateful for the immense response by 150 applicants from all over the continent out of which only 35 were invited due to financial constraints on the workshop budget. We hope this will not deter African scientists in showing interest in this new field of research in the next workshop.

Local Organiser

ACKNOWLEDGEMENTS

The National Organising Committee wishes to express its sincere gratitude to the following:

1. Office of External Activities of International centre for Theoretical Physics (ICTP) and Swedish Agency for Research Cooperation with Developing Countries (SAREC) for the initiation and set up of a Regional Centre at Cape Coast and financial support for holding the workshop.

2. Ministry of Environment, Science and Technology for sponsoring the lodging cost of the workshop.

3. Ghana National Petroleum Corporation for providing funds for transport and accommodation of lecturers and foreign participants as well as the brochures for the workshop.

4. International Commission of Optics (IOC) through whose patronage the Ghana Commission for optics has been born and who also, jointly with ICTP, provided resource persons for the workshop.

5. British Council in Ghana for providing tickets for two lecturers.

6. Association of African Universities, also for providing tickets for two participants from East and North Africa.

7. Costed of West and Central Africa for providing five tickets to participants from West and Central Africa;

8. Ashanti Goldfields Corporation who provided funds to cover stationary, postages, fax, telex and telephone bills;

9. Ghana Cement Company Ltd. (GHACEM) Accra for paying for media announcement of the workshop;

10. P & T Corporation who assisted in the initial planning of the workshop and procurement of conference pads;

11. Society of African Physicists and Mathematicians (SAPAM) for raising funds for the workshop;

12. Pens and Plastics (Gh) Ltd. for providing engraved workshop pens;

13. Fan Milk (Ghana) Ltd. for providing dessert for our meals

14. Astek (Gh) Ltd. for providing some of its products for snacks.

15. Accra Brewery Ltd. for the provision of some products to entertain our lecturers;

16. University of Cape-Coast for hosting the workshop;

17. Prof. F.K.A. Allotey, Course Director and Chairman of Council for Scientific and Industrial Research, and Ghana Atomic Energy Commission through whose untiring efforts the local matching funds were realised;

18. Kerma Carpets for supporting the Workshop;

19. Prof. S.K. Adjepong, the Local Director whose enthusiasm and dynamism have contributed to the success of the workshop;

20. Prof. A.N. deHeer- Amissah, Head of Physics Department and Chairman of the National Organising Committee, all members of the Departmental Board, the M. Phil students and Teaching Assistants of the Department for their willing corporation.

Our special thanks go to all members of the various committee for assisting in diverse ways, the Public Affairs Department of Ghana National Petroleum Corporation for their immense assistance. We express our sincere gratitude to Ms. Gertrude Quansah, Ms. Mercy Yaadar, Mr. Jeff and Ms. Catherine Boison, for secretarial assistance.

UNIVERSITY OF CAPE COAST

PROGRAMME FOR THE THIRD INTERNATIONAL WORKSHOP ON PHYSICS AND MODERN APPLICATION OF LASERS - AUGUST 1994

WEEK 1

TIME	MONDAY (8/8)	TUESDAY (9/8)	WEDNESDAY (10/8)	THURSDAY (11/8)	FRIDAY (12/8)	SUNDAY(14/8)
0830 0900						VISIT TO AKOSOMBO AND ISLANDS
0900 1000		Wave Optics Dainty	Optical Design Maxwell	Basics in Q. Optics Meucci	Non-linear Optics Winful	
1000 1030	FORMAL OPENING	BREAK	BREAK		BREAK	
1030 1130	& INAUGURATION OF GHANA COMMI- SSION FOR OPTICS	Image formaion & Processing - Dainty	Optical Fabrication & Testing- Maxwell	Measurements in Quantum Optics-Meucci	SEMINAR Winful	
1130 1230	(Minister-Environ. Science & Tech)	Fibre Optics - Denardo	SEMINAR Dainty	Non-linear Optics- Brown	Fibre Optics - Brown	
1230 1400		LUNCH	LUNCH		LUNCH	
14000 1500		Fibre Optics - Denardo	SEMINAR Dainty	Non-linear Optics- Winful	Contributed Papers (3)	
1500 1600	Wave Optics - Dainty	Basic in Lasers - Meucci	Visit to Castle	Seminar Maxwell	Contributed Papers (3)	
1600 1630		BREAK	BREAK		BREAK	
1630 1730	Basics in Lasers - Meucci	Geom. Optics - Maxwell	Visit to Castle	Contributed Papers (4)	Contributed Papers (4)	
1830		RECEPTION		CULTURAL NIGHT		

WEEK 2

TIME	MONDAY (15/8)	TUESDAY (16/8)	WEDNESDAY (17/8)	THURSDAY (18/8)	FRIDAY (19/8)
0900 1000	Laser Optics - Seminar Brown	Laser in Industry Asibu	Laser in Medicine Legargasson	Laser in Medicine Legargasson	
1000 1030	BREAK	BREAK	BREAK		
1030 1130	Laser in Chemistry Volpp	Laser in Industry Asibu Seminar	Laser in Environment Kaurenen	Diode Laser Kaurenen	Group Discussion and Conference
1130 1230	Laser in Engineering Asibu	Laser in Chemistry Volpp	Laser in Medicine Legargasson	LAM Discussion	Evaluation
1230 1400	LUNCH	LUNCH	LUNCH		Closing ceremony (1200-1330)
1400 1500	Laser in Industry Asibu	Laser in Environment Kaurenen	Komenda Beach	Seminar Kaurenen	
1500 1600	Laser in Chemistry Volpp	LAFOC and Activities Buah-Bassuah	Komenda Beach	Seminar Kaurenen	
1600 1630	BREAK	BREAK	BREAK		
1630 1730	Telecom 1. Ajayi 2. Thon	Contributed Papers (4)	Komenda Beach	Contributed Papers (4)	
1830 2000				BANQUET (Regional Minister)	

PROGRAMME

MONDAY, 8TH AUGUST, 1994

8.30 - 9.00am.	-	Registration
	-	OPENING CEREMONY - UCC Auditorium Chairman: Prof. F.K.A. Allotey Chairman, International Advisory Board, Laser & Fibre Optics Centre. University of Cape Coast.
9.00 - 9.25am	-	Invited guests proceed to Auditorium
9.25 - 9.35am	-	Introduction of Chairman and Invited Guest: Prof. A.N. deHeer-Amissah Chairman, National Organising Committee.
9.35 - 9.40am	-	Chairman's response: Prof. F.K.A. Allotey
9.40 - 9.50am	-	Vice Chancellor, University of Cape Coast and Local Director of Workshop
10.05- 10.15am	-	Short Address: Prof. G. Denardo Head, Office of External Activities (ICTP) , Trieste, Italy.
4.00 - 4.30pm.	-	Break for Snacks
4.30 - 5.30pm.	-	**LECTURE 2** CHAIRMAN: Prof. S.K. Adjepong SPEAKER: Prof. R. Meucci TOPIC: Introduction to Laser Physics

TUESDAY, 9TH AUGUST, 1994

7.00 - 8.30am.	-	BREAKFAST
		Morning Session CHAIRMAN: Prof. A. N deHeer-Amissah
		LECTURE 3 SPEAKER : Prof J.C. Dainty TOPIC: Image Formation, Storage and Processing.
10.00 - 10.30am	-	Break for Tea
10.30 - 11.30	-	**LECTURE 4** SPEAKER : Prof. G. Denardo TOPIC: Fibre Optics- Fundamentals
12.30 - 2.00pm	-	LUNCH Afternoon Session CHAIRMAN: Prof. Ali Sherif EL-Din
2.00 - 3.00pm	-	**LECTURE 5** SPEAKER: Prof. G. Denardo TOPIC : Fibre Optics - Applications
		LECTURE 6 SPEAKER : Prof. R. Meucci TOPIC: Classification of Laser
10.15 -10.35am	-	Keynote Address: Hon. Dr. C. Amoako-Nuamah Minister of Environment, Science and Tech .
10.35 -10.40am	-	Inauguration of Ghana Commission for Optics Hon. Dr. C. Amoako-Nuamah.
10.40 -10.50am	-	Short Address: Prof. J.C Dainty Immediate Past President, International Commission of Optics
10.50 -10.55am	-	Chairman's Remarks: Prof. F.K.A. Allotey

10.55 - 11.00am	-	Vote of Thanks: Dr. P.K. Buah-Bassuah Coordinator of Regional Optics Centre and Local organiser of Workshop
11.00 - 11.30am	-	Break for Tea
11.30 - 12.15pm	-	Visit to Regional Laser and Fibre Optics Centre
12.15 - 1.15pm.	-	Activities of the Ghana Institute of Physics.
1.30 -3.00pm.	-	Lunch Afternoon Session
3.00 -4.00pm.	-	**LECTURE 1** CHAIRMAN: PROF. F.K.A. Allotey SPEAKER : Prof. J.C. Dainty TOPIC: Diffraction and Polarisation
4.00 -4.30pm	-	Break for Snacks
4.30 -5.30pm	-	**LECTURE 7** CHAIRMAN : DR. P.K. Buah-Bassuah SPEAKER : Prof. J. Maxwell TOPIC : Geometrical Optics : Basics in Optical Engineering.
5.30 -6.30pm	-	BREAK
6.30 -8.00pm.	-	RECEPTION

WEDNESDAY, 10TH AUGUST, 1994

7.00am- 8.30am	-	BREAKFAST Morning Session CHAIRMAN: Dr. A.V. Gholap
9.00 - 10.00am	-	**LECTURE 8** SPEAKER : Prof. J. Maxwell TOPIC : Optical Design & Fabrication

11.30 - 12.30pm - **SEMINAR 1**
SPEAKER : PROF. J.C. DAINTY
TOPIC : Adaptive & Atmospheric Optics

12.30 - 2.00pm - LUNCH

2.00 - 3.00pm - **SEMINAR 2**
CHAIRMAN: Prof. A. Wague
SPEAKER : Prof. J.C. Dainty
TOPIC: Measurement of Surfaces

3.00 - 5.00pm - Visit to Cape Coast Castle
Dr. Haruna Yakubu (Leader)

THURSDAY, 11TH AUGUST, 1994

7.00 -8.30 - BREAKFAST

Morning Session 1

CHAIRMAN: DR. S.Y. Mensah

9.00 - 10.00am - **LECTURE 8**
SPEAKER : Prof. R. Meucci
TOPIC: Noise Phenomena and Chaotic Instabilities.

10.00 -10.30am - Break for Tea

10.30 -11.30am - **LECTURE 9**
SPEAKER : Prof. R. Meucci
TOPIC: Detection of Optical and InfraRed Radiation.
Morning Session II
CHAIRMAN : Prof. J.C. Dainty

11.30 - 12.30pm - **LECTURE 10**
SPEAKER : Prof. C. Brown
TOPIC: Polarisation Phenomena in Optical Fibres 2.30-

12.30 - 2.00pm - LUNCH

Afternoon Session I

2.00 - 3.00pm - **LECTURE 11**
CHAIRMAN: Prof. J.C. Dainty
SPEAKER : Prof : H. Winful
TOPIC : Optical Phenomena - Solitons

Afternoon Session II

3.00 - 4.00pm - **SEMINAR**
CHAIRMAN: Prof. G.O. Ajayi

10.30 - 11.30am - **LECTURE 14**
SPEAKER : Prof. J. Maxwell
TOPIC : Optical Testing.

4.00 -4.30pm - Break for Snacks

4.30 -5.30pm - Presentation of 4 Contributed Paper
CHAIRMAN: Dr. G.O. Ajayi

5.30 -6.30pm - BREAK

6.30 -8.00pm - CULTURAL NIGHT
Dr. Haruna Yakubu **(Leader)**

FRIDAY 12TH AUGUST, 1994

7.00 -8.30am - BREAKFAST

Morning Session

CHAIRMAN: Prof. R. Meucci

9.00 -10.00am - **LECTURE 12**
SPEAKER : Prof. H. Winful
TOPIC: Non - linear Dynamics of Coupled Lasers

10.00 - 10.30am - Break for Tea

10.30 - 11.30am - **SEMINAR 4**
SPEAKER : Prof. H. Winful
TOPIC: Non-linear Dynamics of Coupled Lasers

11.30 - 12.30pm - **LECTURES 13**

SPEAKER : Prof. H. Winful
TOPIC: Fibre Optics Devices

12.30 -2.00pm - LUNCH

Afternoon Session I

Presentation of 8 Contributed Papers
CHAIRMAN: Dr. T. Gasmi

4.00 -4.30pm - Break for Snacks

Afternoon Session II

4.30 -5.30pm - Presentation of 4 Contributed Papers
CHAIRMAN : Dr. S.M. Chagwedera

SUNDAY, 14TH AUGUST 199

6.00 -6.30am - BREAKFAST

6.30 -5.00PM - A trip to Akosombo Lake and Islands

WEEK TWO

MONDAY , 15TH AUGUST,1994

7.00 -8.30am - BREAKFAST

Morning Session I

9.00 -10.00am - **SEMINAR 5**
CHAIRMAN: Prof. H. Winful
SPEAKER : Prof. C. Brown
TOPIC : Optical Fibre Applications.

10.00 -10.30am - SNACKS

Morning Session II

10.30 -11.30am - **LECTURE 14**
CHAIRMAN : Prof. B.A. Dadson, Head, Chemistry Dept., UCC, Cape Coast.
SPEAKER: Dr. H.R. Volpp
TOPIC: Laser in Chemistry

11.30 -12.30pm - **LECTURE 15**

CHAIRMAN : Prof . J . Maxwell
SPEAKER : Prof. Kannatey- Asibu
TOPIC : Laser Welding

12.30 -2.00pm - LUNCH

Afternoon Session I

2.00 - 3.00pm - **LECTURE 16**
CHAIRMAN: Mr . F. Baffoe- Eshun
SPEAKER ; Prof. Kannatey-Asibu
TOPIC: Laser machining

3.00 - 4.00pm - **LECTURE 17**
CHAIRMAN: Dr . V.P.Y. Gadzekpo
SPEAKER : Prof. H.R. Volpp
TOPIC: Laser in Chemistry

4.00 - 4.30pm - SNACKS

4.30 - 5.30pm - **SEMINAR 6**
CHAIRMAN: Mr. Asibu
Regional Director, P&T Corporation,
Cape Coast.
SPEAKERS :1. Dr. G.O. Ajayi
2. Dr. G.N. Thon
TOPIC : Laser in Telecommunication

TUESDAY, 16TH AUGUST, 1994

7.00 -8.30am - BREAKFAST

Morning Session I

9.00 - 10.00am - **LECTURE 18**
CHAIRMAN: Mr P.K. Mensah
SPEAKER: Prof . Kannatey-Assibu
TOPIC : Laser Heat Treatment

10.00 - 10.30am - SNACKS

10.30 - 11.30am - **SEMINAR 7**
CHAIRMAN : DR. Haruna Yakubu
SPEAKER : Prof Kannatey-Asibu
TOPIC : Laser Material Processing

11.30 - 12.30pm - **LECTURE 19**
CHAIRMAN : Mr. C Entsuah-Mensah
SPEAKER : Dr. H. R. Volpp
TOPIC : Laser in Chemistry

12.30 - 2.00pm - LUNCH

Afternoon Session I

2.00 - 3.00pm - **Lecture 20**
CHAIRMAN : Dr. E.C. Quaye
SPEAKER : DR. P. Kaurenen
TOPIC : Monitoring of Atmospheric Pollutants.

3.00 - 4.00pm - TALK: LAFOC and Activities
CHAIRMAN : Mr G. K. Quainoo
Dr. P.K. Buah-Bassuah

4.00 - 4.30pm - SNACKS

Afternoon Session II

4.30 - 5.30pm - Presentation of 4 Contributed Papers
CHAIRMAN : DR. F.S. Tayman
Chemistry Dept. , UCC, Cape Coast.

WEDNESDAY, 17 TH AUGUST, 1994

7.00 - 8.30am - BREAKFAST

Morning Session I

9.00 - 10.00am - **LECTURE 21**
CHAIRMAN : Prof. C. Ameyaw-Akumfi
Pro-Vice-Chancellor, UCC. , Cape Coast.
SPEAKER : DR. Jean-Francois Legargasson
TOPIC : Laser Velocimetry in Medicine

10.00 - 10.30am - Break

10.30 - 11.30am **LECTURE 22**
SPEAKER : Dr. Legargasson
TOPIC : Laser Opthalmology

11.30 - 12.30pm - **LECTURE 23**
SPEAKER : Dr. P. Kaurenen
TOPIC : Medical Diagnostics

12.30 - 2.00pm - LUNCH

Afternoon Session

2.00 - 5.00pm - A visit to Komenda Beach
Dr. Haruna Yakubu (Leader)

THURSDAY, 18TH AUGUST, 1994

7.00 - 8.30am - BREAKFAST

Morning Session

9.00 - 10.00am - **LECTURE 24**
CHAIRMAN : Dr. S.O. Fiakpony
Director of Medical Services,
UCC HOSPITAL, Cape Coast.
SPEAKER : Dr . Jean-Francois Legargasson
TOPIC : Laser Surgery

10.00 - 10.30am - LAM Discussion
CHAIRMAN : Dr. P.K. Buah-Bassuah

12.30 - 2.00pm - LUNCH

Afternoon Session I

2.00 - 3.00 pm - **SEMINAR 8**
CHAIRMAN : Dr. D.K. Dodoo
Chemistry Dept., UCC, Cape Coast.
SPEAKER : DR. P. Kaurenen
TOPIC: Monitoring Vegetation with Laser

3.00 - 4.00pm - **SEMINAR 2**
CHAIRMAN : Dr. S.M. Gueye
SPEAKER : DR. Jean-Francois Legargasson
TOPIC : Laser in Medicine

4.00 - 4.30pm - SNACKS

Afternoon Session II

4.30 - 5.30PM - Presentation of 4 Contributed Papers
CHAIRMAN : Prof A. Barhdadi

6.30 - 8.00pm - BANQUET

FRIDAY, 19TH AUGUST , 1994

7.00 - 8.30am. - BREAKFAST

Morning Session

8.30 - 9.30am - Presentation of 3 Contributed Papers
CHAIRMAN : Prof A.N. deHeer-Amissah,

9.30 - 11.30am - Group Discussion and Conference Evaluation
CHAIRMAN : DR. P.K. Buah-Bassuah

11.30 - 12.00noon - SNACKS

CLOSING CEREMONY

	-	CHAIRMAN: Prof. C. Ameyaw-Akumfi Pro-Vice-Chancellor, UCC.
12.00 - 12.10pm	-	Introduction of Chairman: Mrs. Irene Annor-Frimpong
12.10 - 12.15pm	-	Chairman's Opening Remarks
12.15 - 12.25pm	-	Short Address: Prof. A. Wague, LAM President
12.25 - 12.35pm	-	Short Address : Prof. P.K. Buah-Bassuah ICAC Project
12.35 - 1.00pm	-	Address: Hon. Mr. E.K. Fosu Ag. Regional Minister, Central Region
1.00 - 1.25pm	-	Chairman's Closing Remarks
1.25 - 1.30pm	-	Vote of Thanks - Mr. P. K. Mensah.
1.30 - 2.30pm	-	Lunch

SATURDAY, 20TH AUGUST , 1994 - **DEPARTURE**

RELATIVISTIC EFFECT ON WAVE GENERATION BY LASER-PLASMA INTERACTION IN AN OSCILLATING INHOMOGENEOUS MAGNETIC FIELD

SH.M. KHALL, Y.A. SAYED and Kh. H. EL-SHORBAGY

Plasma Physics Dept.
Nuclear Research Centre
Atomic Energy Authority
Cairo-Egypt.

ABSTRACT

Non linear wave generation has been recently the subject of many studies due to its importance in plasma diagnostics techniques, studying the interaction of intensive electromagnetic wave with plasmas, and others. In particular, the investigation of the interaction of light waves (lasers) with surface waves in a plasma present a special interest when considering the stability of devices based on the use of charged particle beams and also in connection with the appearance of new methods for optical spectroscopy of condensed media intended for research on surfaces, interfaces, and thin films (e.g. [1,2] and references cited there.)

Generation and radiation of electromagnetic waves at combined frequencies and second harmonics due to nonlinear plasma interaction has been investigated by many authors, either for isotropic (e.g. [3,4] or anisotropic plasma ([5-7]). In the latter, the system is non-relativistic and the plasma was placed in a static spatially homogeneous external magnetic field.

When the external magnetic field oscillates at a high frequency, the corresponding wavelength becomes much smaller than the other scale length of the system, and it will be more realistic to take into consideration the spatial inhomogeneity associated with the oscillation of the magnetic field. In fact this is important from the practical stand point, when the electron displacement from equilibrium position is considerably less than the characteristic scale of the magnetic field inhomogeneity.

Besides, in the presence of strong magnetic field, interaction of relativistic incident radiation with a plasma have attracted interest in connection with higher energy deposition in various devices for intense electromagnetic radiation generation.

Accordingly, in this paper we consider these new effects on the wave generation of waves at combined frequencies and second harmonics. A relativistic P-polarised light wave with a frequency ω_1 is obliquely indecent from vacuum on a thin inhomogeneous plasma layer

of width (d) to pump a S-polarised surface wave propagates, with a frequency ω_2, on the vacuum-plasma boundary. An inhomogeneous external magnetic field oscillates at frequency ω_m ($H_{ext} = e_z H_0(X) \exp(-i\omega_m t)$) perpendicularly directed to the direction of the gradient of the unperturbed plasma density $n_0(X)$, is considered. $n_0(X)$ is an arbitrary function of x in an inhomogeneous thin plasma layer ($0 \leq x \leq d$) and equal to zero at $x \leq 0$ and $x \leq d$. We assume that wavelengths are much greater than the width of the plasma layer ($\lambda \ll d$, $(\omega_{pe} d/c) \ll 1$). These conditions enables us to find solutions for the fields in the inhomogeneous plasma layer.

Different cases are investigated, the wave generation at both (i) second harmonics, $2\omega_1$ and $2\omega_2$, and (ii) combined frequencies, $\omega_1 + \omega_2$. The external magnetic field is assumed to oscillates at arbitrary frequencies; i.e. at $\omega_m = \omega_1, \omega_2, 2\omega_1, 2\omega_2, \omega_1 = \omega_2$. We calculate the current density, electric and magnetic field components and the amplitudes for both the fundamentals and generated waves.

Generally speaking, oscillation and inhomogeneity of external magnetic field, relativistic effect, and type of polarisation of interacting waves are found to play an important role in connection to the amplification or damping of the generated waves.

References:

1. V.M. Agranovich and D. L. Mills (eds.), Surface Waves Polarisation: Electromagnetic Waves of Surfaces and interfaces, Elsvier, New York (1982).

2. A.A. Zharov, Sov. J. Plasma Physics, 16 (1990) 184.

3. A.R. Barakat, V. V. Dolgopolov and N.M. El-Siragy, Plasma Physics, 17 (1975) 89.

4. N.M. El-Siragy, Sh. M. Khalil, W.H. Amein and O.Z. Nagy Plasma Physics, 23 (1981) 1189.

5. V.V. Dolgopolov, N.M. El-Siragy and Y. A. Sayed, 7th European Conf. on Controlled Fusion and Plasma Phys. 1-5 Sept., Lausanne, Switzerland (1975).

6. Sh. M. Khalil, I. A. El-Naggar, Y.A. Sayed and R.N. El-Sherif, Physica Scripta, 30 (1985) 357.

7. Sh. M. Khalil, I. A. El-Naggar, Y.A. Sayed and R.N. El-Sherif, Int. J. Theor. Phys. 24 (1985) 1001

CONSTRUCTION OF A NITROGEN LASER FOR PLASMA DIAGNOSTICS

GEORGE J. ISHIEKWENE

Department of Physics
College of Science and Technology
University of Liberia
Monrovia, Liberia.

ABSTRACT

The challenge faced in finding new sources of energy to bridge the gap between the availability and demand of energy is difficult to be overemphasised. Nuclear fusion seems to provide a potentially limitless source of energy which offers a bright prospect for solving this problem.

Although an elaborate programme in fusion may be beyond the economic reach of most third world countries, some modest experiments are necessary to provide an indigenous expertise capable of enhancing international fusion studies.

In order to initiate experimental research sufficient for plasma studies at an affordable cost for developing countries, this paper illustrates the construction of a simple, low cost, high power Nitrogen laser and investigates some of its performance characteristics. Also, the laser is utilised in studying the dynamics of a spark plasma using techniques of shadow grams depicting the temporal development of the plasma discharge is realised.

The constructed laser is found to be cost-effective useful in small-scale researches in laser-plasma diagnostics.

BINDING ENERGY CHANGES IN SQUARE CROSS SECTION GaAs/GaAlAs

QUANTUM WELL WIRE AND APPLICATIONS TO ADVANCEMENT OF LASER TECHNOLOGY

MBUGUA ZAKAYO

Department of Physics
Moi University, Kenya.

ABSTRACT

Numerical simulations of impurities in a GaAa/GaAlAs quantum well wire of square cross section and the carrier binding have been done. These calculations were done for both hydrogenic and non hydrogenic cases for donor impurities. In both these cases the binding energy was found to be enhanced as the physical size of the wire was reduced. This phenomena imply that semiconductor micro structures can now ;be tailored to get the desired properties by quantum confinement which is the actual reason for this binding energy change exhibited by quantum well wires as well as related structures called quantum wells and quantum dots. Moreover the enhanced binding energy implies that scattering by ionised impurities is reduced and hence a reduction of electrical resistance. A qualitative discussion of the excited states and a reference to the applications in laser technology has also been given.

CIRCULAR POLARISATION OF LINE RADIATION EMITTED FROM HI-LIKE IONS FOLLOWING IMPACT EXCITATION BY LONGITUDINALLY POLARISED ELECTRONS

M. K. INAL

Institut des Sciences Exactes
Department de Physique
Tlemcen, Algeria.

ABSTRACT

In the excitation of ions by an electron beam that is spin-polarised, the collision strength for transition to the different magnetic sublevels of a level depends on the absolute value of the magnetic quantum number but also upon the sign. The radiation subsequently emitted in the decay of such level exhibits not only linear polarisation but also circular polarisation of X-ray lines produced by highly charged ions which are collisionally excited by a longitudinally polarised beam of electrons is theoretically considered. A distorted-wave program has been used to calculate the required collision strengths for exciting the individual magnetic sublevels of the target ion. The relativistic interactions are taken into account as perturbations through the Breit-Pauli approximation. The calculations carried out for the He-like ions with no nuclear spin predicted that the resonance line labelled w due to the 1^1S_o - 2^1P_2 transition is very weakly circularly polarised. But the three lines labelled x, y, and z due to the 1^1S_o - 2^3P_2 magnetic quadruple transition, 1^1S_o - 2^3P_2 intercombination transition, and 1^1S_o - 2^3P_2 magnetic dipole transition, respectively, can have a high degree of circular polarisation reaching values of about 60 to 96% for He-like ion in the near-threshold region. For scandium which is monoisotopic with nuclear spin I = 7/2, it is found that the hyperfine interaction has a strong circular depolarisation effect on the lines x, y and z. Being of great interest for atomic collision physics, the obtained results may stimulate experimentalists into performing measurements of circular polarisation in the X-ray range.

A COMPUTER SIMULATED OPTICAL SPECTROSCOPY OF A THIN METAL FILM

METAL FILM IN KRETSCHMANN PRISM-METAL FILM-AIR CONFIGURATION

SHIMELES ASSEFA

Kotobe College of Teacher Education
Addis Ababa, Ethiopia.

ABSTRACT

In this paper a relatively original theoretical account of the optical properties of a thin metal film in Kretschmann structure is presented. Unlike for an unsupported ($\varepsilon_3 = \varepsilon_1$) film no analytical splitting of the dispersion equation has been found for the supported ($\varepsilon_3 \neq \varepsilon_1$) film in the limit of very small thickness [1]. Thus, a numerical method of solving the thin film dispersion equation for the latter case is developed. The existing surface plasmon polaritons method for the determination of complex dielectric permittivity and thickness of metal film, is reviewed. A close electrodynamic analysis of surface plasmon polaritons dispersion properties in very thin metal film is made.

The analysis is based on the numerical solution of th exact dispersion equation using th 'Downhill' simplex method and subsequent selection of physically reasonable results. The selection is performed via the comparison or continuity of the power flows through the boundaries of the metal film in the transverse direction. The simulated laser light that is made incident on the structure is that of He-Ne laser, $\lambda \equiv 0.63$ μm. The parameters chosen are thickness h= 800Å; relaxation time $\tau = 10^{-13}$ s; ε_1 (air) = 1; ε_3 (prism) = 2.25; and ωp (plasma frequency) = 10^{15} Hz. The results obtained are compared to the case of unsupported film, which is already well studied [1], [2], with the same choice of parameters. The analysis of results showed that splitting of the classical thin film dispersion equation into two branches (ω^-(lower) mode and ω^+(upper) mode) known in literature, [2], [3], for the case of unsupported film occurs also for the case of supported film when numerical solutions of th dispersion equation is plotted, but the ω^+ mode branch is represented by a number of discrete points only. The existence of long-range (ω^+) surface mode for a film in surrounding media of slightly different ($\varepsilon_3 \approx \varepsilon_1$) dielectric constants has experimentally been confirmed for almost all values of ε_{2r} and ε_{2i} [4]. In order to check the validity of the results explicit expressions for the

components of the power flow in both of the supported and unsupported film structures have been derived and plotted. The study of physically significant results revealed back-bending segments in the ω^- and ω^+ branches which demonstrate the phenomena of artificial anomalous dispersion. Therefore, the results of spectroscopy of surface plasmon polaritons can be employed in developing new optical methods for investigating surfaces and thin films.

References:

1. D. Sarid: Phys. Rev. Lett. 47, 1927 (1981)

2. H. Raether: Springer Tracts in Modern Physics Vol. III, Springer-Verlag, Berling Heidelberg, 1988.

3. V. M. Agranovich, D.L. Mills (Eds.) Modern Problems in Condensed Matter Sciences, North Holland Publishing Company, 1982.

4. F. Yang, J.R. Sambles, and G.W. Bradberry: J. Mod. Opt. (UK), Vol. 38, No.4, p. 707-17 (1991).

RING FABRY-PEROT INTERFEROMETER FOR SEMICONDUCTOR LASERS LINEWIDTH MEASUREMENT

KEDRO DIOMANDE

Physieque Universite Nationale d'Abidjan
Abidjan, Cote D'ivoire

ABSTRACT

Using Fabry-Perot interferometer to measure semiconductor linewidth is some time difficult because of feedback effect.

To overcome this problem, we realise a ring Fabry-Perot interferometer which main characteristics are presented in this paper and also its application on measuring linewidth extended cavity and distributed feedback lasers.

USING LASERS AS A BETTER TRANSFORM MODULE

G. ANENE

Department of Physics and Industrial Physics
Nnamdi Azikiwe University, Awka, Nigeria

ABSTRACT

This paper examines a new paradigm in laser technology. We have studied the diffraction pattern produced by single and multiple slits as well as measured the reflection coefficient for a glass plate. Our analysis model reveals an accurate value for the measurements and further portrays the use of lasers as a more efficient analysis of various transforms in preference to computers

LASER INDUCED THERMOELECTRIC EFFECT

S. Y. MENSAH, A.N. DEHEER-AMISSAH AND J. KUTOR

Department of Physics, University of Cape Coast
Cape Coast, Ghana.

ABSTRACT

The effect of laser on non-parabolic (kane) semiconductors have been theoretically studied. The kinetic equation for no equilibrium distribution function as a result of the presence of laser field has been solved. We predicted the existence of new photo current and density of heat flow which depend on the direction of the laser.

INDUCED PHOTOCONVERSION EFFECT OF CH_2DCH_2D BY CO_2 LASER

RITA KAKOU YAO

Physique Universite Nationale d'Abidjan
Abidjan, Cote D'Ivoire

ABSTRACT

The spectroscopy of 1,2 D_2 Ethane. (CH_2DCH_2D) shows that we have two symmetry; Left form (C_2) and trans (anti) form (C_{2h}).

All vibrations modes of left form are actives in middle infrared region particularly, in matrix of xenon, V_{12B} mode of molecular with CO_2 laser transition P_{20} (00°-1-02°0).

This irradiation shows a photoconversion left ↔ trans due to photon absorption.

THE TURBIDITY OVER CAIRO

T. N. EL. HOSARY

Physical Research Department
Egyptian Meteorological Authority

ABSTRACT

A new technique for measurement of turbidity by using the MAINZ-SUNPHOTOMETER M-11 which is a precision electro - optical device, enabling the determination of the aerosol optical thickness with 5 interference filtered centred at 368,500,675,778,862 nm and a bandwidth between 2nm and 5nm are carried out at Cairo.

The aerosol optical depth τ_A (λ) at specified wavelength λ have been studied for all seasons, the maximum was observed in spring and summer and the minimum was in clear sky days in winter.

MOLECULAR SPECTROSCOPY-LARGE BASIS FOR REMOTE SENSING OF ATMOSPHERIC POLLUTION AND GENERAL METEOROLOGICAL CONDITIONS

NZOHABONYO PIERRE

University of Burundi
Bujumbura, Burundi.

ABSTRACT

Remote sensing techniques are becoming increasingly important for monitoring the state of the Earth's atmosphere. Weather conditions and atmospheric pollution are of great interest for both global and local monitoring. The remote-sensing observations can perform from the ground or from air - or spaceborne platforms. Atmospheric monitoring is largely based on Molecular Spectroscopy, and in this paper we will discuss the basics interactions between radiation and matter are reviewed as a background for a description of different spectroscopic methods, useful for remote sensing applications.

A distinction is made between passive and active techniques. In the former type of technique the spectral distribution of the background radiation is utilised in absorption-emission-or reflection measurements. Although image-forming passive registrations in selected wavelength bands such as photography or area-scanning from weather or land resources are very important we will not consider this kind of remote sensing here, but will rather concentrate on spectroscopic methods which employ dispersive, Fourier instruments in absorption or emission measurements.

We will examine the results of spectral analysis of the boron diatomic compounds and we will discuss the implication of the Na in the pollution of the upper Atmosphere. Lidar measurements for this purpose will be chosen as a topic for a somewhat detailed discussion.

COHERENT OPTICAL PROCESSOR - A GENERATOR OF HIGH FREQUENCY GRATINGS

DR. SINGH SHYNM

Department of Physics
University of Zambia, Lusaka

ABSTRACT

Coherent optical processing and its applications have been described by (1-5) in detail. Perhaps the most important applications of holography are holographic interferometry and holographic gratings. In this paper, we describe a technique for making gratings of higher frequencies. This is achieved by selecting and filtering only particular set of spatial frequencies displayed in the filtering plans. A plane phase grating is require only as an object in a coherent optical processor. By this technique, a large number of grating structures in a single exposure can also be produced.

Reference:

1. L. Mertz, Transformation in Optics, Wiley, New York 1965.

2. R. J. Collaier, Optical Holography, Academic Press, New York, 1971.

3. H. Lipton, Optical Transform, Academic Press, London, 1972.

4. W.T. Cathey, Optical Information Processing and Holography, John Willey & Sons Inc. New York 1974.

5. M. Born and E. Wolf, Principles of Optics, Pergamon Press, Oxford (1975).

INDICATIONS OF PULSED DYE LASER LITHOTRIPSY IN THE TREATMENT OF URETERAL CALCULI

S. M. GUEYE, C. SYLLA, A. NDOYE, M. BA, A. MENSAH

Department of Urologic Surgery
Dakar-Etoile, Senegal

ABSTRACT

Patients with ureteral stones may be managed expectantly or treated with a variety of invasive or non invasive techniques depending on stone's chemical composition, size and localisation.

Unfortunately, in our developing countries, surgical ureterolithotomy remains the only mean applicable to our calculi according to the rarity or absence of modern technologies, while, elsewhere, Endoscopy and Extracorporeal Shock Waves lithotripsy (E.S.W.L.) had modified ureteral stones therapeutic strategies.

More recently, during last few years, Pulsed Dye lasers has been developed and proposed in the treatment of ureteral stones.

This new device has the usual characteristics of pulsed dye lasers for the fragmentation and destruction of lithiasis.

The pulsed dye laser emitting at wavelength of 504 nm, for 1 msec, at a frequency of 5 to 20 Hz, is transmitted via a 250 µm, in diameter optic fibre. This optic fibre is passed into the ureter through the working channel of a 9.5 F rigid ureteroscope. The intervention is performed under general anaesthesia. The wavelength of 504 mn corresponds to the optimal wavelength of light absorption by the calculi, without absorption by surrounding tissues, particularly ureteric wall.

The main indication of pulsed dye laser lithotripsy is treatment of lumbar ureteral calculi. It could also be indicated for partial fragmentation of solid or impacted symtomatic stones of any localisation in the ureter. Afterward, the fragments are extracted by Dormia Catheter of flushed in the pelvis kidney. In this case, fragmentation is completed by Extra Shock Waves Lithotripsy. Rare complications as ureteral perforation or hemorragia has been reported. They are due to ureteroscopy rather than the pulsed dye laser. The ability to use miniaturised ureteroscopes reduces the difficulties of ureteroscopic access and complications.

In conclusion, lithotripsy of ureteral calculi by Pulsed Dye Laser constitutes progress in the treatment of ureteral calculi. The absence of tissue damage, and the flexibility and small diameter of the laser fibre allow this technique to be used at all levels of the ureter with extremely low risk of complication.

COMPUTER MODELLING OF SIMPLE OSCILLATORY AND OPTO-ELECTRICALLY INTEGRATED NITROGEN GAS LASER CIRCUITS

A. V. GHOLAP AND M. MATHUTHU

Department of Physics
University of Zimbabwe, Harare

ABSTRACT

The paper describes computer modelling of simple oscillatory circuit. The extension of this model to an opto-electrically integrated transversely excited nitrogen gas laser circuit is used to evaluate important parameters of the laser such as power absorbed by the laser and the variation of the voltage, current and rate of increase of the laser gap voltage. The use of normalised non dimensional equations used for the analysis enables one to change the parameters of the circuit with varied values and facilitates optimisation procedure. The results for a critically damped opto-electrically integrated nitrogen laser circuit are discussed.

PRELIMINARY DESIGN OF A LONGITUDINAL FLOW CO_2 LASER

COSMAS CHITEME

Department of Physics,
University of Zimbabwe
Harare, Zimbabwe

ABSTRACT

The preliminary design of a continuous wave longitudinal flow carbon dioxide lase using a mixture of CO_2, He and N_2 at a pressure of 15 torr will be presented. A double-jacketed tube of length 60cm and internal diameter of 1.5cm will be used. With water as a coolant, the expected output power is 30W.

This electrode material will be platinum wire in order to avoid oxidation at high pressure which normally occurs with copper electrodes. The rear mirror is coated Gold on Silicon and Zinc Selenite as the output mirror. The design of the associated High Voltage Power Supply [10 kv dc, 0-40mA] will also be presented. Most of the material to be used in the construction will be locally available, hence the laser should be affordable to many educational institutions.

MEASUREMENT OF VISCOSITY BY DAMPED MECHANICAL OSCILLATIONS OF A PLUNGER

P.K. BUAH-BASSUAH, ASAMOAH BOSOMTWI, AND P.K. MENSAH

Department of Physics,
University of Cape Coast,
Cape Coast, Ghana.

ABSTRACT

An Experimental investigation of the measurement of viscosity by making use of the damping of mechanical oscillations by a viscous fluid is presented. The principle depends on a plunger being vibrated is sensed by another transducer by means of resonance. The coefficient of viscosity is evaluated from its direct relation with the change in the amplitude. This method has been applied less viscous fluids and heavy fluids of various mixture compositions. Possible trails have been made using laser to enhance the amplitude of the sign.

LIGHT SCATTERING AT FLUID INTERFACE FOR SURFACE TENSION MONITORING

P. K. BUAH-BASSUAH, P. K. MENSAH AND G. ASIEDU AMANKWAH,

University of Cape Coast.
Cape Coast, Ghana.

ABSTRACT

Waves that appear on liquid surfaces may be subjected to ransom disturbances caused by surface tension forces. These forces are monitored when the air-water; and air-monolayer-water interface is excited by a needle driven by a loud speaker which is triggered by a low signed generator to generate cylindrical waves.

The interception of these waves by a 5 mW HeNe laser beam produces diffraction patterns on a screen. Analysis of these patterns give quantitative measure of surface tension forces on ideal fluid (air-water) or molecular monolayer film on the ideal fluid (air-monolayer-water). Measurements were made with various fluids of different orders of viscosity coefficient.

PROSPECTS OF LASERS IN ENVIRONMENTAL NOISE POLLUTION STUDIES

DR, M. U. ONUU

Department of Physics
University of Calabar,
Calabar, Nigeria,

ABSTRACT

The technique of laser-probing of the atmosphere (acoustic path) or lidar measurements in the Source-path-Receiver system has revealed possible applications of lasers in Environmental Noise Pollutions (ENP) studies. Discrete measurements separated by days and collected over a period of months or years can be used for the detection of "shadow zones" and other areas where the equivalent noise Level, $L_{eq} = L_{eq}^*$ or minimum . This is a place where, for example, a not yet existing hospital could be located or cited. This will, among other things, reduce the rate of medical consolation by psychiatric patients especially. In general, the description presented in this paper should be useful for the solution of noise control problems, in town and country planning. It could also be used as a guide in making decisions about noise laws, ordinances and other governmental acoustical matters especially for areas where aircraft noise dominates the noise climate.

FIBRES FOR OPTICAL COMMUNICATIONS

D. ODHIAMBO AND D. O. OMING'O

Department of Telecommunications Engineering
Kenya College of Communications Technology
Nairobi - Kenya.

ABSTRACT

The main types of optical fibres that are extensively used in signal transmission are presented, their relevant optical characteristics discussed and future prospects outlined. Light propagates in a fibre in accordance with the laws of reflection and refraction. Although these laws have been known for centuries, serious attempts to send communication signals through fibres began only in the seventies. Today, fibres dominate the long distance point-to-point cable links and are networks. The reasons for their tremendous expansion are their advantages as compared to metallic wires and particularly the combination of low attenuation and high bandwidth characteristics.

CHARACTERISTICS OF SOURCES AND DETECTORS FOR OPTICAL FIBRE COMMUNICATIONS

D. O. OMING'O

Department of Telecommunications Engineering
Kenya College of Communications Technology
Nairobi - Kenya

ABSTRACT

Various optical sources and detectors that are extensively used in fibre optic communication are discussed with a view to high - lighting their electrical and optical characteristics, and practical limitations. The electronic circuits that are used to drive them are presented and their (sources/detectors) interactions with the fibre explained.

DETERMINATION OF MASS TRANSFER COEFFICIENT IN TWO-PHASE BUBBLY FLOW USING LASER-DOPPLER ANEMOMETRY

DR. ENG. K.M.A. KASSEM

Mech. Power & Energy Department
Faculty of Engineering & Technology
Minia University
Minia, Egypt

ABSTRACT

In the last two decades, numerous research works have been conducted about the utilisation of Laser-Doppler Anemometry (LDA) as a new technology in a great numbers of engineering and scientific measurements. Reported data concerning measurements of thermal and fluid flow parameters showed a very high degree of reliability when using LDA in comparison with results of other classical or traditional techniques. In the field of two-phase bubbly flow, LDA is considered to be ne of the most significant and helpful tools in obtaining the flow parameters experimentally with minimum measuring errors. For gas bubbles rising in liquids, in the present study, the bubble size and its velocity are simultaneously determined using low-power He-Ne Laser-Doppler Particle Analyser.

This paper is concerned with th advanced application of laser technique to two-phase bubbly flow in order to determine the mass transfer coefficient from the acquired experimental parameters. Therefore, this study is undertaken to develop a calculational procedure for predicting mass transfer relations in bubbly liquid column, which is the configuration most common in industrial and mechanical engineering processes.

The purpose of this paper is to present typical example of using laser technology in order to provide a framework for the detailed understanding of two-phase bubbly flow mass transfer mechanism. Results using the LDA technology are also compared with those of other techniques reported in literature.

EBIC QUANTITATIVE MAPPING USING SEM IMAGE PROCESSING

A. BARHDADI[1], J. L. MAURICE[2], M. RODOT[3]

1. **Laboratoire de Physique des Semiconducteurs et de l'Energies Solaire P:S:E:S:), Ecole Normale Superieure de Takaddoum, BP 5118, Rabat - Morocco.**

2. **Laboratoire de Physique des Materiaux (L:P:M:), C.N.R.S., 1-Place A, Briand, F-92195, Meudon-France.**

3. **Laboratoire de Physique de Solide de Bellevue (L.P.S.B.) C.N.R.S., 1-Place a. Braind, F-92195, Meudon-France.**

ABSTRACT

Electron Bean Induced Current (EBIC) in the Scanning Electron Microscope (SEM) is a well adapted technique for the study of recombination phenomena in semiconductor devices. It can be employed in various forms to measure the minority carrier diffusion length. However, the local aspect of the measurements is best preserved in the method using the variation of beam energy. The collecting junction must be parallel and closer to the surface; it may be either a Schottky barrier or a p-n junction. the variation of th collection efficiency with the kinetic energy of the incident electrons has been model takes into account the minority carrier diffusion length (L_D) in the bulk, the recombination rate (V_{sn}) in the Space Charge Region (SCR), and the lifetime (τ_p) in the superficial n region of the p-n junction.

The SEM used in part of a fully computerised system equipped with softwares that permit data collection and visualised image-processing on screen. The facilities of this system have been exploited to calibrate the 256 (2^8) gray levels of an EBIC image and to express them in terms of collection efficiency (η) and diffusion length L_D. Hence, the L_D mapping gives the experimental values of this parameter at each pixel; i.e. 512 x 512 data points for each EBIC image can be obtained.

In this paper, we use this system to characterise high efficiency solar cells (2cm x 2cm), made on multicrystaline silicon (POLIX) material, using a new technology [2]. The quantitative mapping allows one to characterise very small local variations. Moreover, recording maps at different beam energies permits to differentiate bulk and surface contributions to the overall efficiency. For instance, we observed very high recombination

velocities ($V_{sn} \cong 10^6 cm.s^{-1}$) in zones of relatively large diffusion length ($L_D \cong 100\ \mu m$), while in contrast, a very small recombination rate ($V_{sn} < 10^4 cm.s^{-1}$) was recorded in regions containing a high density of recombinant grain boundaries and having a lower diffusion length ($L_D \cong 70\mu m$). On the other hand, the cells with high collection efficiency generally present large values of τ_p.

References:

1. J. L. Maurice, J. Phys. 111, France 3 (1993)

2. J. Nijs, M. Ghannam, J. Coppye, G. Palmers Le Quang Nam, M. Robot, So. Sivoththaman, S. Sarti and R. Perruzzi, 11th European Photovoltaic Solar Energy Conference, Montreux, October, 1992.

DEMONSTRATING THE 'BEAT' PHENOMENA WITH LASER TACHOMETER: COMPUTER SIMULATION

M. S. ABUBAKAR

College of Science & Technology
Kaduna, Nigeria.

ABSTRACT

The 'beat' phenomenon occurs when two wave trains of the same amplitude and slightly different frequencies interfere, thus producing a resultant wave whose amplitude varies in intensity with the maxima ('beat') occurring with the periodicity of the frequency difference. This phenomenon is easily demonstrated acoustically by sing two tuning forks of early equal frequencies, but visual demonstration is usually indirect by superposing alternating voltages in the oscilloscope, whereby the oscillatory nature of the combining signals, though visible, is not easily conceived from first principles.

In this work varying electrical signals are produced by reflecting lase light from a rotating cylinder having reflecting and absorbing sectors alternated on its surface. The cylinder has two segments of different diameters so that a laser beam, split by means of a half-silvered mirror, is separately reflected from the two segments and recombined at a photoelectric detector to give an interference of two signals of slightly different frequencies but nearly equal amplitudes. Equality of patterns on the two segments. Frequency difference arises only form the difference in segment diameters. The output of the detector can be observed acoustically by using a loudspeaker or displayed visually on the oscilloscope screen. In this arrangement the origin of oscillations is obvious.

The first part of the project reported here consists of computer simulation suing typing parameters, while the second will involve a practical demonstration using an electric motor to rotate the cylinder and a low power He-Ne laser as light source. The Metrologic calibrated photometer catalogue Number 60-230 serves as the photo-electric detect.

THE PROPAGATOR FORMULATION OF LIGHT EMISSION BY TWO-LEVEL ATOMS

FESSEHA KASSAHUN

Department of Physics
Addis Ababa University
Addis Ababa, Ethiopia.

ABSTRACT

The statistical properties of the light emitted by N two-level atoms initially in the initially in the upper level is analysed employing the coherent-state propagator. We strongly believe that the propagator formulation provides a convenient means of investigating the quantum dynamics of a system. We describe the system of interest by a quantum Hamiltonian exclusively expressed, using the Schwinger representation of angular momentum, in terms of bosom operators. Since it is impossible to obtain an exact expression for the associated propagator, the operator in the Hamiltonian representing the atoms in the upper level is replaces by a c-number function.

The propagator can be determined applying path integral methods or by directly solving the Schroedinger equation. However, we realise that the propagator is expressible in terms of the c-number function corresponding to the evolution operator for the normal ordering. It thus proves to be convenient to evaluate the propagator by solving the equation of evolution for this c-number function.

Finally, by means of the resulting propagator, we calculate the mean and variance of the photon number. We also present a systematic derivation of the photon number and photon count distributions. Our analysis shows that, consistent with the conclusion drawn by other authors, the emitted light is chaotic.

AN EXPERIMENTAL LIDAR SYSTEM FOR MONITORING THE CLOUDS BASE HEIGHT AT C.D.T.A. LASER LABORATORY

T. GASMI, R. KASBADJI, R. BOUSHAKI, S. BOUDJEMAI, A. OUNIS

Solid State Laser Group, Laboratory of Lasers
Centre de Development des Technologies Avancees: C.D.T.A.
BP 245, Chemin Med Gacem, El Madania,
Algeirs, Algeria.

ABSTRACT

Lidar systems are used for atmospheric probing for man years and the advances in electro-optical technology now permit the development of such systems with a very broad range of capabilities for making quantitative measurements of the atmosphere. Lidars operate as optical frequency radars in which short, intense lase pulses are transmitted into the atmosphere and receivers are used to collect and analyse the backscattered signal.to derive information about the atmosphere. By making use of variety of scattering and absorbing processes it is possible to obtain information about the atmosphere, its constituents and their changes in both space and time.

Within the C.D.T.A. laser laboratory a demonstration lidar system has just been built. This is a Nd:YAG based lidar that would measure the Rayleigh and Mie scattering at two wavelengths and is capable of detecting the backscattered signal. This lidar system is being used in the troposphere to measure clouds base height and their vertical structure.

The lidar employs a laboratory made Nd:YAG laser source and is operated at 10Hz. The output energy is 200mJ. The beam is steered vertically upwards into the atmosphere by a simple beam-steering prism. The backscattered radiation is collected with a 20 cm objective and sent via a telescope and an interference filter (λ = 1.06 μm) onto the active surface of an avalanche photodetector (RCA 30556). The APD is directed to a 250 MHz digital oscilloscope via a high speed low noise linear amplifier stages.

PARTICLE SIZING WITH MIE SCATTERING

P. K. BUAH-BASSUAH, MOSES JOJO EGHAN

**Department of Physics, University of Cape Coast,
Cape Coast, Ghana.**

ABSTRACT

An unexpanded 5mW He Ne laser is incident on a cell containing the sample solution. The angular distribution of light scattered intensities in the main lobe of the Fraunhoffer diffraction pattern produce from the cell changes rapidly with particle size which is independent of its refractive index. The experimental arrangement of this device is described and the evaluation of the particle sizes explained. Samples of homogeneous latex spheres of diameter 2,9 μm were used to standardise the device whilst measurements were made on Kaolin Clay and Cement powder samples suspension.

PARTICLE SIZING OF VIBRATING POWDERY CLAY SAMPLE BY DOUBLE-EXPOSURE SPECKLE PHOTOGRAPHY

P. K. BUAH-BASSUAH, ERIC AMPEM-LASSEN

Department of Physics, University of Cape Coast, Cape Coast, Ghana.

ABSTRACT

An experimental investigation of monitoring the sizes of vibrating powdery clay sample is being presented. The method of double-exposure speckle photography is used to determine small displacements of the powdery sample. The diffused glass plate was illuminated by 5 mW He-Ne laser light and speckle pattern was recorded on a stationary holographic plate twice, once before and once after the sample had been vibrating with the speckles. The developed photographic plate is illuminated with unexpanded laser beam to produce interference fringes on the Fraunhofer diffraction plane which are then analysed. The spacing and the orientation of the fringes is determined to enable the size of the powdery sample to be evaluated. This method is found to be essential since it is a non contact and hence non-destructive testing.

GEOMETRICAL OPTICS AND THE SPECIFICATION AND DESIGN OF IMAGE FORMING OPTICAL SYSTEMS

J.Maxwell
Applied Optics Section,Imperial College, London

The primary purpose of geometrical optics is to provide the tools to enable us to design optical equipment. Every piece of optical equipment has to be designed and as in all engineering design there are many important details which have to be considered; it is the purpose of this course to introduce you to some of these details and to the concepts and techniques which are used in optical design, more particularly lens design.

The Applied Optics section at Imperial College was set up in 1917 because there were no national facilities for training in optical design; now, 70 and more years later, training and research in optical design is still a key part of our function as a group within the Physics department, and in this respect we are different to the rest of the Physics department, because we provide specific vocational training in this way.

We can identify the critical sequence of activities in optical design:

(a) The development of the complete instrumental concept and the specification of its performance requirements.

(b) The specification of the requirements for individual subassemblies based on a thin lens layout. This step involves the choice of either reflecting or refracting systems and the consideration of telephoto and inverse telephoto effects.

(c) The application of Seidel and other algabraic methods to the preliminary aberrational design of the individual subassemblies. This step mainly involves paraxial and thin lens concepts but there are also some noteable starting points which do not require these restrictions.

(d) The choice of practical component thicknesses and appropriate diameters to establish a starting prescription.

(e) The balancing of primary aberrations against higher order aberrations using differential correction techniques without restriction to thin lens or paraxial concepts. It is at this stage that decisions are also made about the application and balancing of vignetting effects.

(f) The optimization of the balanced design to achieve lower aberration residuals.

(g) The repeat of steps (c)-(f) as required.

(h) The consideration of diffraction effects in the aberrations of the optimum design and the making of minor adjustments to the aberration balancing taking account of these effects.

(i) The preparation of the final design prescription for manufacture: Tolerancing, the fitting of standard manufacturing surface radii and the accountancy of any specific glass refractive index values for the meltings that are to be used.

OPTICAL FABRICATION AND TESTING

J.Maxwell
Applied Optics Section, Imperial College, London

Optical instruments are expensive precision products and the user expects to be able to rely absolutely on the quality of the images formed.

To satisfy this requirement the manufacturer has to invest considerable effort in tolerancing and specialist quality control techniques. The history of the development of optical instrument manufacture has been characterised by the close collaboration between the engineers involved in the activities of design, manufacture and test. Each new advance in design specification has had to be followed by the development of appropriate techniques for manufacture and test.

In the case of optical instruments manufactured in large quantities, the requirements of optical quality can present the manufacturer with some particularly difficult quality control situations where especially precise components are required and unless appropriate tolerancing, production and testing techniques exist a satisfactory product cannot be delivered to the customer.

As an example of this situation we may consider the case of roof prisms where considerable economies of bulk may be achieved by using a 90 degree feature between two polished faces which split the optical aperture. Such prisms require the 90 degree roof angle to be good to within a few seconds of arc (1 second of arc = 1/3600 of a degree!). This is shown in fig.1. To manufacture such prisms in production quantities has required the development of special tooling techniques which utilise optical contacting methods on master 90 degree blocks, which are themselves worked and maintained to even finer tolerances.

OPTICAL DESIGN AND TECHNOLOGY: A KEY DISCIPLINE FOR INSTRUMENTATION

J.Maxwell
Applied Optics Section, Imperial College, London

ABSTRACT: Many instrumentation situations use optical techniques. This paper is a brief review of the extent of application of these techniques, followed by an example of a contemporary design problem, the design of the zoom lens for a large format theatre projector.

I INTRODUCTION

Photography, astronomy, microscopy,photogrammetry, metrology, refractometry,polarimetry,interferometry reprography, holography, television,spectroscopy..... The list is almost endless. All these techniques lean heavily on optical instrumentation, which in turn is dependent on optical design and manufacturing.

Central to the power of optical techniques is the mechanism of image formation and we shall restrict ourselves in this paper to a discussion of optical instruments that form images in the conventional sense.

II THE NATURE OF OPTICAL DESIGN AND TECHNOLOGY

Each development in computational mathematics has been seized on by the optical design community as the answer to their prayers. The design of image forming systems requires a level of numerical work which is quite exceptional and traditionally optical designers have spent a large proportion of their professional lives wrestling with pages of numbers. With this background it is hardly surprising that optical designers are such enthusiastic computer users.

The other aspect of optical instrumentation that concerns us here is the manufacture of lens components and the mechanical mountings which hold them. These manufactured components will often be made in large quantities for a very modest unit cost using equipment which covers the range from simple pieces of cast iron and pitch, through to numerically controlled diamond surfacing machine tools which represent a major capital investment.

The simple,spherically surfaced lens component is an example of the very highest levels of dimensional and geometrical accuracy. The polished surfaces of such a component are worked to a radius of curvature which may be controlled to an absolute accuracy of .01% and a relative accuracy of perhaps one fifth or even one tenth of this, The spericity is also controlled to within similar limits, as is the surface texture of the polished surfaces. The colinearity of the optical and mechanical centre lines is guaranteed to within a few microns by the use of special optical centration techniques.

The optical glass of which such lens components are made is similarly a precision product, which bears only a superficial similarity to it's poor cousin, window glass. The absolute refractive index of optical glass is controlled to better than .00050 and the homogeneity is controlled to better than one fifth of this figure or better. Unfortunately the processing properties of optical glass frequently leave a great deal to be desired and many optical glasses are more like soft crystals than hard gems with the exception of their prices which follow the opposite trend.

The final vacuum-evaporation surface treatments which are designed to frustrate surface reflections are also a carefully refined and highly sophisticated aspect of modern lens manufacture which result in transmission levels well in excess of 99% for each individual lens component. These thin film dialectric stacks may consist of 5 or more films which are applied with the greatest possible attention to thickness control, uniformity, cleanliness and adhesion. This requires specialist electrophotometric measuring instruments and microprocessor controlled vacuum equipment if an adequate control is to be exercised over the final performance of the films.

The finished optical components are frequently assembled in groups of 6 or more and a complex zoom lens may have as many as 20 optical components (see Fig 1). These assemblies have to be held in a mechanical mounting so that the optical axies of the individual lens components are held colinearly to within a few microns. In a zoom lens this colinearity has to be maintained while the

zooming components are moved to adjust the final focal length of the complete lens.

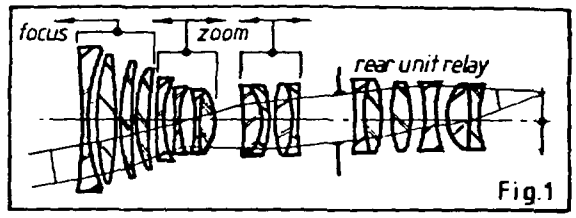

Fig.1

III REPRESENTATIVE OPTICAL SYSTEMS

Most optical systems have a circular aperture which defines the ultimate microscopic structre of the images formed. In particular, a spatial impulse (point source), when imaged by an optical system which has a circular aperture produces an image which is not a point source but the celebrated Airy diffraction pattern, which in cross section has an intensity defined by

$$I(y') = \left[\frac{J_1(y')}{(y')}\right]^2 \qquad \ldots\ldots\ldots\ldots\ldots\ldots (1)$$

where y' is given by

$$y' = \frac{6.2815\, n' \sin u'}{\lambda}\, r$$

n' being the refractive index of the medium in which the image is formed, u' is the semi angle of the cone of the rays forming the image, λ is the wavelength of the light and r is the radius in the diffraction pattern, measued in the same units as the wavelength. $J_1(y')$ is the Bessel function of the first kind with argument y'. This intensity distribution is shown in Fig 2.

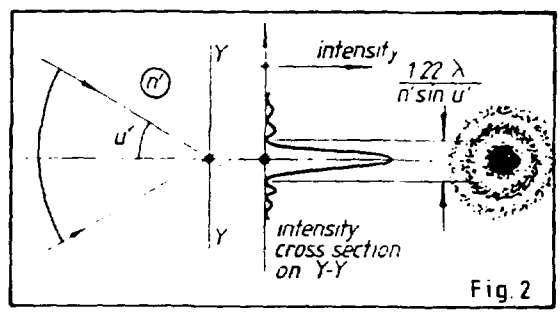

Fig. 2

The astronomical telescope and the microscope are capable of working close to the limit of resolution set by this diffraction pattern. In the case of these instruments, resolution is expressed in terms of the minimum separation of two point image diffraction patterns at which there is a just detectable dip in the intensity between the two central maxima. In the case of instruments which are free of aberration this minimum separation is the radius of the central maximum.

For photographic systems where the spatial bandwidth is limited to frequencies less than 60 or 70 c/mm, the diffraction limit of resolution set by the diffraction pattern shown in Fig 2 is usually irrelevent and the criterion of image quality is taken to be the contrast characteristic of the image of a sinusoidal spatial grating as shown in Fig 3. Bearing in mind that an f/2 photographic lens has a diffraction limited bandwidth of 909 c/mm at a wavelength of 550 nm, it is clear that only a small proportion of the diffraction limited bandwidth is of importance in photographic image assessment.

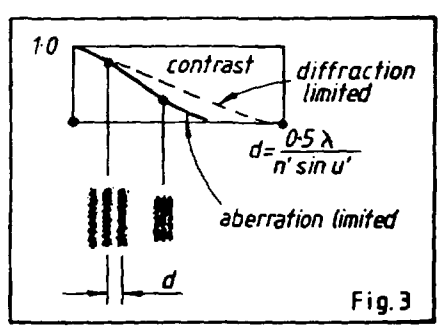

Fig. 3

Television systems are very similar to photographic systems, but a 2/3" television tube which has an image circle of 11 mm diagonal is only intended to work out to a spatial frequency of 30 c/mm, although high resolution television will work with a double bandwidth, that is, to a spatial frequency of 60 c/mm.

The teoretical optical design task associated with an astronomical telescope is not dissimilar to that associated with the design of a microscope and indeed, the resolution potential for these instruments is expressed by equation 1 in both cases. Thus, in principle, we could use an astronomical telescope

as a microscope by projecting enlarged images of microbes into outer space - we could even perhaps use the moon as a screen if we had a bright enough light source! Conversely, we could make a very large microscope objective and use it as an astronomical telescope, but of course such a design choice would lead to financial disaster.

IV MAXIMISING THE INFORMATION CONTENT OF OPTICAL IMAGES

The information technologist or the systems engineer may require to know how many bits of information an optical system can handle, and clearly, if the resolution limit of the lens - film combination is 60 c/mm, it means that in a square mm of image area such a combination can contain a black and white checkerboard 120 elements square (one "cycle" = 1 black element plus 1 white element) or 1.4×10^4 bits. Thus, in a standard 35 mm still frame which is 24 mm x 36 mm we would have a total of 1.2×10^7 bits.

Such terminology may be familiar to the systems engineer, but the optical engineer is interested in the localised variation of resolution or image modulation, which is dependent on the state of aberration correction of the lens forming the image and the quality of its construction.

In particular, at the specification and design stage, it is the well known optical aberrations which are the optical engineers concern: Spherical aberration, coma, chromatic aberrations, astigmatism, field curvature and distortion. With the exception of distortion each of these aberrations can drastically reduce the resolution capabilities of an optical system in whichever region of the image they occur Distortion is an image degredation which corresponds to a different type of information loss.

At the construction stage, the optical engineer is concerned with the realisation of the optical prescription defined by the optical designer. Errors of curvature, component separation or refractive index, represent a modification of the design intention, but there are also a whole family of constructional errors which lead to the image plane being tilted, or a comatic or astigmatic caste being applied to the whole image. For example, if an optical surface is polished so that it has slightly different curvatures in different sections through the centre of the lens, then the focal length will be different in different sections of the lens and this results in an astigmatic caste across the whole image. If one of the surfaces of a lens is tilted due to inaccurate edge grinding then the image surface will be tilted with respect to the optical axis, with the result that the resolution level recorded in the detector plane will only be acceptable along one line in the field of view, that line which is the intersection of the detector plane with the tilted image.

The determination of manufacturing tolerances prior to manufacture is a vital step in the production of optical instruments, and it is probably the least well understood aspect of optical engineering. There are two types of tolerance to be determined: tolerances which are applied to features which do not perterb the rotational symmetry of the system and tolerances which are applied to features which can (and do !) perterb the rotational symmetry. The former catagory of tolerances are relatively easy to determine and statistically rationalise, but the latter catagory of tolerances present formidable problems to the optical design engineer. The statistical behaviour of complex assemblies of defective components is not well understood in the context of the radial vectorial nature of their effects. Fig 4 shows a comparison between two different lens constructions in terms of their tolerance sensitivity and statistical characteristics. The four component (Tessar) lens has 7 optical surfaces, 6 of which are air-glass and one of which is glass-glass; this results in the ill-balanced radial vectorial summation of image tilts (or astigmatic contributions) shown in the corresponding vector diagram. The 6 component (Double Gauss) lens has 10 optical surfaces of which two are glass-glass; this results in a much better behaved vectorial distribution of errors, as shown.

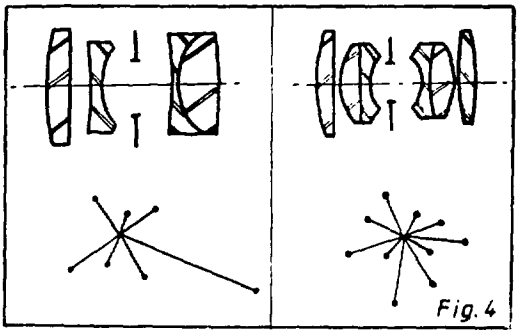

Fig. 4

In a practical lens assembly the vectorial summation represented by Fig 4 will not of course be evenly distributed in azimuth and there will frequently be azimuthal "bunching" as a result of some mechanical shoulder being out of square or a particular stock of glass components being built up of a "wedged " lens.

V THE OPTICAL DESIGN OF A SPECIFIC OPTICAL SYSTEM

As in many other specialist engineering disciplines, the novice worker in optical design is ofter not aware of the key literature references - these references are frequently out of print and the copy belonging to the library has sometimes mysteriously disappeared, but the fact is that optical design has a relatively rich book literature (1-9) and a lively literature in many current international journals.

We shall examine now the techniques of optical design involved in the design of a zoom projection lens. I have chosen this particular project as being representative of the type of optical design work that is going on in industrial design offices in the 1980's and which is only scantily discussed in the literature (Ref 6, p60; Refs 10 and 11). I shall strip the calculations to their most simple essence in an attempt to clarify and interesting and topical subject. In particular there are certain features of the design process which are unique to zoom lenses and which are conceptually extremely elementary, but without which it is not possible to procede with the design work in a systematic and convergent fashion; I shall try to emphasise these features.

The system we shall consider is required for theatre background projection purposes. The focal length range is 220mm - 500mm covering a slide diagonal of 225mm with an aperture of f/2.8 at f = 220mm and an aperture of f/4 at 500mm. We are thus talking about an intrinsically very large lens and it will be necessary for it to be as simple as possible and for it to be made from inexpensive optical glass or plastic.

The configuration chosen for this lens as the simplest type of mechanically compensated two-component zoom converter placed in front of a rear unit projection objective. The projection objective can be considered as consisting of two lenses: a lens to afocalise or collimate the image for the zoom section (that is, to turn the zoom section into a telescope) and a collimating lens focussed on infinity to project the slide through the telescope. This conceptual layout is shown in Fig 5, along with the prefered position of the aperture stop. The stop positioned at the interface of the projection lens and the zoom converter ensures that the entrance pupil of the total projection lens will remain constant during zooming.

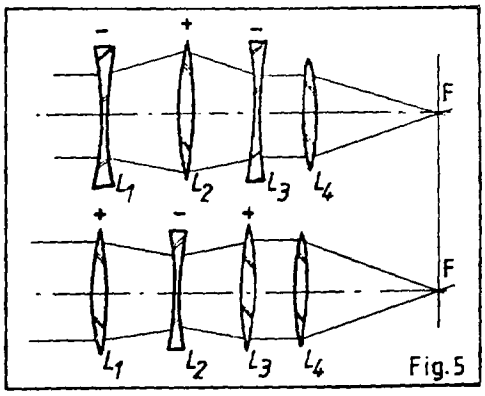

Fig.5

Alternative configurations that have the advantage of simplicity for the zooming mechanism are the family of optically compensated zoom lenses; these use the simple ganged motion of two or more optical subassemblies to achieve the variation of focal length. Simple as the zoom mechanism of these lenses is, they are generally 1.5 to 2.0 times as bulky as the equivalent mechanically compensated systems; this can actually be an advantage for short focal length systems but it is quite unacceptable in the present applcation. Another difference between optically and mechanically compensated systems is the variation of focal regisration that is inevitable in optically compensated systems; this would not preclude their use in the present application but it is an unattractive feature which causes trouble in lenses with large zoom ratios or where the focal lengths covered are long compared with the format size.

We may now procede to design our zoom system in two halves: first the zoom telescope, with a constant aperture and a field view defined at the aperture stop and secondly the objective designed to compensate the aberrations of the zoom section and project the object slide of the specified size.

The step by step design is then as follows·

1) Provisional thin lens design

a) zoom ratio = $Z = \frac{500\ mm}{220\ mm} = 2.27273$

b) The most compact zoom section telescope has a magnification range of $\sqrt{Z} = 1.50756$ to $1/\sqrt{Z} = 0.66332$.

c) If the zoom converter telescope has a magnification of 1.50756 when the overall lens has a focal length of 500 mm, then the projection lens (L_4) must have a focal length of 331.66 mm. or to check, consider the short focal length end:

$$331.66\ mm \times 0.66332 = 220mm$$

d) At f = 500 mm overall focal length, the relative aperture is f/2.8, so the stop diameter is

$$331.66mm/2.8 = 118.45\ mm.$$

e) Set the relative aperture of the afocalising lens (L_3) to f/6. This is a completely arbitrary choice which will be revised as required. Although this initial choice is arbitrary it has far reaching consequences because it sets the scale of the telescopic zoom adaptor, which in turn determines the level of aberration which has to be stabilised in the telescope and which is the inverse of the aberration which has to be projected into the zoom converter by the projection lens.

This choice gives $f_3 = \pm 118.45\ mm \times 6 = \pm 710.7\ mm.$

f) Set $f_1 = f_3 = \pm 710.7$ mm.

g) When the two zooming components are coincident, at the end of the lens furthest from the slide, the axial marginal ray height leaving the telescope will be

$$\frac{118.45\ mm}{2} \times 1.50756 = 89.285\ mm$$

or

$$\frac{118.45mm}{2} \times 0.66332 = 39.285\ mm$$

depending on whether $f_1 = f_3$ is negative or positive, as shown in Fig 6.

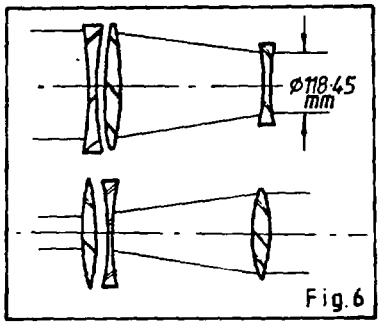

Fig.6

For simplicity we shall now abandon one of these two alternatives, again reserving the right to reverse the decision in the light of subsequent aberrational developments. The solution we shall reject will be the + - + configuration, on the basis that our specification has a relatively wide angular field of view and the - + - configuration is more obviously inverse telephoto than the + - + configuration.

So the ray height leaving the projector for the axial pencil is 89.285 and thus the combined focal length of the front two lenses of the zoom telescope attachment is:

$$f_{1+2} = \frac{89.285\ mm}{59.225\ mm} \times 710.7\ mm = 1071.42\ mm.$$

but having selected $f_1 = -710.7$ mm we can see that:

$$f_2 = \frac{1}{\frac{1}{f_{1+2}} - \frac{1}{f_1}} = 427.28\ mm$$

and the length of the zoom telescope is

$$L_{NA} = \left|f_{1+2}\right| - \left|f_3\right| = 360.72\ mm$$

where the subscript NA implies "Narrow Angle".

h) From the symmetry of the telescope we can see that when its magnification is x1 its length will be

$$L_{MZ} = 2(2 \times \left|f_2\right| - \left|f_3\right|) = 287.72\ mm$$

where the subscript MZ implies " Mid Zoom". Thus the position of L_1 has changed by

$$287.72\ mm - 360.72\ mm = -73mm.$$

i) Again from considerations of symmetry we can see that when the telescope magnification is 0.66332 it is merely the inverse of the arrangement at the magnification of 1.50756 and

$$L_{WA} = 360.72 \text{ mm}$$

where the subscript WA inplies "Wide Angle"

j) We may now review the basic structure of our thin lens layout for three zoom positions NA, MZ, and WA. These three zoom positions are shown in Fig 7. Note that the central positive lens moves a total of 360.72 mm while the front negative lens only moves in and out by 73 mm so we may regard L_2 as doing the focal length changing and L_1 as the focussing trimmer.

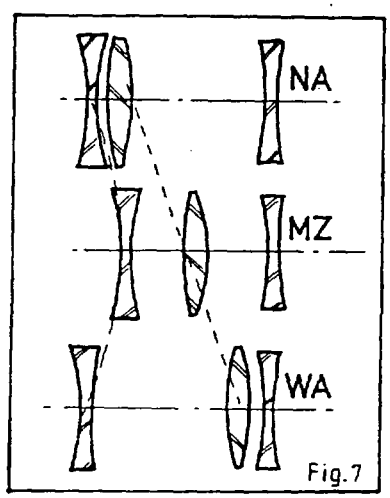

Fig.7

k) As the final step of the thin lens layout we must notice that when we thicken up the lens components it will not be possible for L_2 to travel the full 360.72 mm of its required travel because it would crash into L_1 at NA and L_3 at WA, so we must reduce the focal lenghths of L_1 and L_3 and move them outwards by the same amount as we reduced their focal lengths, so giving more clearance for L_2.

STEPS a - k ABOVE COULD BE WRITTEN DOWN ON THE BACK OF AN ENVELOPE (OR TWO!) BUT IT IS A VITAL RULE OF ZOOM LENS DESIGN THAT YOU MUST BE ABLE TO FEED BACK INFORMATION TO ANY STAGE OF THE CALCULATION AND THEN RECOMPUTE ALL THE SUBSEQUENT STAGES TO SEE WHAT EFFECT IT HAS ON THE ABERRATIONAL STABILITY OF THE DESIGN. TO THIS END IT IS VITAL THAT THE ABOVE THIN LENS LAYOUT WORK IS CLEARLY DOCUMENTED.

2) Thickening up

a) Having calculated the individual focal lengths we may now trace a paraxial thin lens ray out from the edge of the stop at the appropriate paraxial field angle which is :

$$\frac{\frac{225\text{mm}}{2}}{f_4} = .3392 \text{ (radians)}$$

The purpose of this ray is to locate the edge of each of the two zoom components at each zoom position so that the maximum required component diameters may be selected. Again, this ray tracing should be carefully documented because at a later stage in the design process it is usually expedient to introduce vignetting which economises on lens diameters and trims off aberrations.

b) Single components or compound lens subassemblies may now be roughed-out as starting points for the differential correction stage of the design work. These rough designs should only be "rough" in terms of their aberration correction. As far as their focal lengths are concerned they should be scaled precisely to the required value in each case and the resulting positions of the nodal points taken into account when the thick lens components are fitted onto the thin lens skeleton.

In the case of our lens the scale of the beast requires that we attempt to use single components for the zooming section, and following intuition we may choose a crown glass for the positive zooming component and a flint glass for the negative component, by so doing we build a partial measure of chromatic correction into the design.

For simplicity we also choose to make L_1 plano-concave and L_2 equi-convex, more or less on the basis of intuition.

This results in the telescope design shown in Fig 8 which has the stability of aberration correction shown on the right hand side of the diagram (in arbitrary units).

c) There now comes a particularly important stage: The aberration stability graphs shown in Fig 8 are unacceptable and it is necessary to achieve much smaller variations of aberrations. For this design improvement process to be meaningful it is vital that the focal lengths and the nodal point positions of the modified components are kept rigidly in their correct relative positions, otherwise the iterative design improvement process can diverge very rapidly. It is this requirement that separates zoom lens design from conventional lens design and it involves the use of carefully planned analytical algebraic thick-lens modification routines which achieve these requirements.

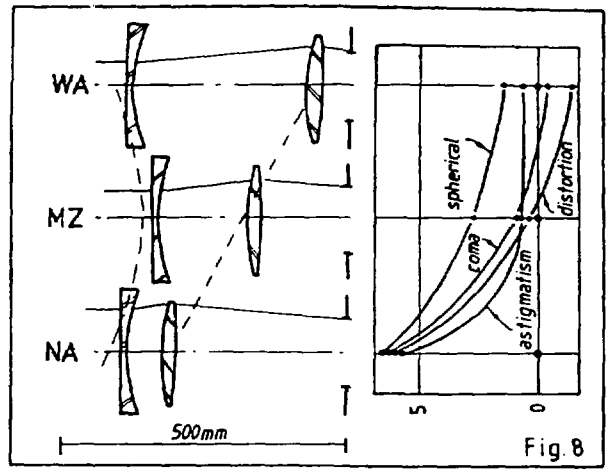

Fig. 8

Fig 9 shows the result of carefully executed differential correction. The aberration graphs are to the same scale as in Fig 8 and the aberration differences that were controlled in optimisation are marked. The optimisation in this case was carried out on a small programmable calculator, but there is no reason why large scale optimisation programs shouldn't be "tricked" into doing this work

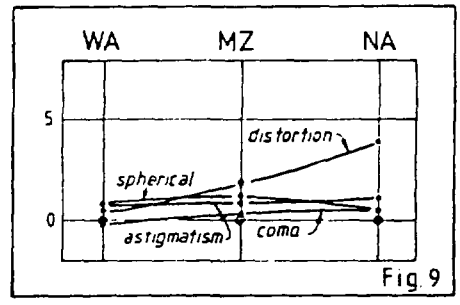

Fig. 9

3) Thin lens structural modifications

Having designed the best possible telescope based on a particular thin lens construction it is now possible to survey the effects of changing the thin lens structure by repeating all the stages described so far with a different scale of telescope or with a zooming motion which is not symmetrical. This process can consume a great deal of time and effort and it is important that it is carefully controlled, documented and reviewed if one is not to lose ones way.

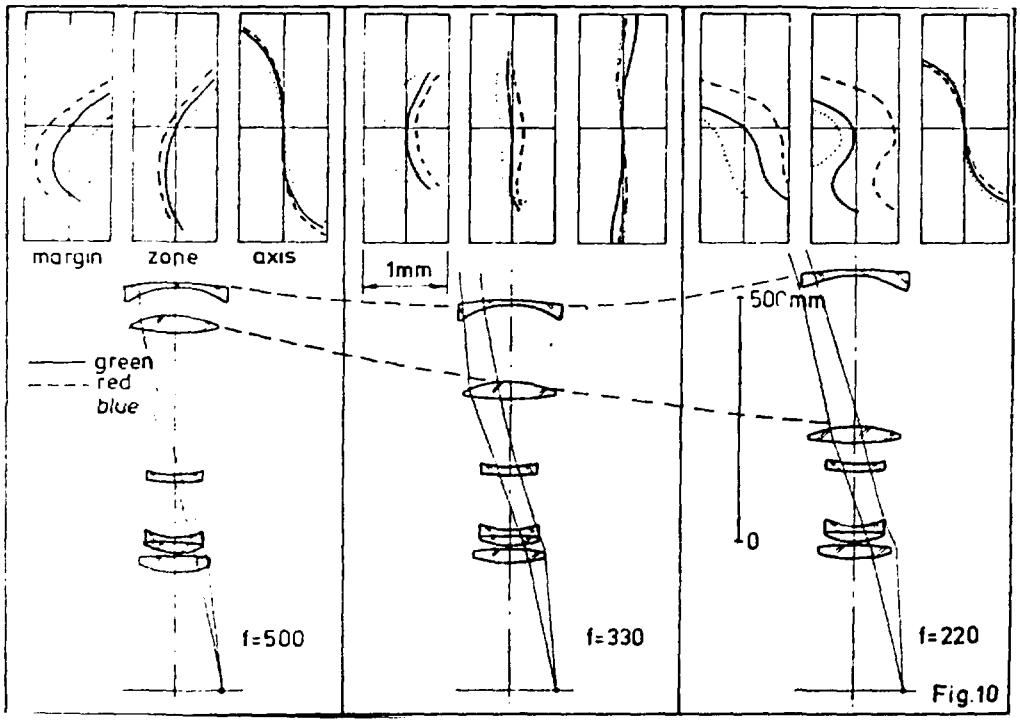

Fig.10

4) Thick lens structural modifications.

We arbitrarily chose thick lenses of particular glass types. A thorough design survey will of course require a systematic consideration of different simple and compound thick lens starting points for each of the zooming components.

5) Projection lens design.

Having satisfied oneself that one has achieved an optimum telescope design which is characterised by, above all, stability of aberration correction at the stop, it only remains to design the projection lens which has exactly equal and opposite aberrations at the stop.

Figure 10 shows the construction and aberration correction of the final design of projection lens.

REFERENCES

1 Conrady A.E. Applied optics and optical design. Vol 1. Oxford 1929 Reprinted by Dover 1957.

2 Conrady A.E. Applied optics and optical design. Vol 2. Dover 1957

3 Cox A. A system of optical design. Focal Press 1964.

4 Hopkins H.H. Wave theory of aberrations. Oxford 1950.

5 Jacobs D.H. Fundamentals of optical engineering. Mc Grawhill 1943.

6 Kingslake R. Lens design fundamentals. Academic Press 1978.

7 Smith W.J. Modern optical engineering. Mc Grawhill 1966.

8 U.S. Defence Supply Agency Military standardization handbook. Mil HDBK 141: Optical design.

9 Welford W.T. Optical design, Chapter 4 in "A guide to instrument design". Taylor and Francis 1963.

10 Yamaji K. Design of zoom lenses. Chapter IV of Progress in optics Vol VI. 1967.

11 Kingslake R. The development of the zoom lens. J. SMPTE 69 p534 - 544. 1960.

Acknowledgements

It gives me particular pleasure to be able to thank the directors of J.H. Dallmeyer for permission to publish this paper.

Thanks are also due to Mr. M. Salter of the Salter Optical Consultancy for many fruitful and stimulating discussions held under such convivial circumstances in the years 1979-81.

Last but by no means least my wife Janet who typed this manuscript and suffered the usual privations of a marriage partner under such circumstances deserves more than the usual measure of praise.

Ultra sensitive gas detection using frequency modulated diode lasers

Peter Kauranen and Sune Svanberg
Department of Physics, Lund Institute of Technology,
P.O. Box 118, S-221 00 Lund, Sweden

Introduction

In the last decade great efforts have been invested into developing and characterising frequency modulation (FM) techniques employing frequencies far up in the megahertz region. This has improved the value of laser absorption spectroscopy for trace species detection significantly. Although a variety of FM methods exist, fundamentally they are variations of the same technique. Common to the different approaches is the shifting of the detection band to high frequencies to avoid laser source (1/f) noise. The absorption signal is homodyne detected, either on the same frequency as the applied modulation frequency, an overtone or an intermediate frequency. FM techniques in the kilohertz region are often referred to as wavelength modulation spectroscopy (WMS). When the applied modulation frequency is comparable with the halfwidth of the absorbing molecules or larger one talks about frequency-modulation spectroscopy (FMS).

The basic principle of FMS is as follows: When a laser is frequency-modulated principally two optical frequency sidebands are generated on the laser beam. These sidebands, separated from the optical carrier by a frequency equal to the modulating frequency, are equal in magnitude but opposite in phase. The amplitude modulation (AM) arising from the beating of the upper sideband against the carrier, perfectly cancels the AM arising from the lower sideband beating against the carrier. When the frequency-modulated laser beam is obstructed by a spectral feature, the sidebands will be differentially absorbed, giving rise to an amplitude modulation, beating at the modulation frequency. Using a photodiode, reacting fast enough for the modulation frequency, the beat notes can be detected and through conventional radio frequency (RF) technique, be demodulated to a signal directly proportional to the differential absorption of the sidebands.

Since linewidths of atmospheric gases often are several gigahertz, a comparable detection bandwidth can be difficult to implement. Detection of gigahertz frequencies requires a detector and detection electronics of comparable bandwidth, which increases price and limits the experimental convenience. Two-tone frequency modulation spectroscopy (TTFMS) has been developed to avoid some of these difficulties [1,2]. Using two closely spaced modulation frequencies ($\nu_m \pm 1/2\Omega$), sideband pairs are generated on the laser beam. In TTFMS a wide frequency separation between the sideband pairs is preserved, but the detection frequency is shifted to a lower and technically more easy manageable frequency regime. The detection frequency will be the frequency difference between the two modulation frequencies, often selected in the frequency region 1-10 MHz. One practically important advantage of two-tone over single-tone FMS is that in TTFMS the signal is recovered at a frequency (Ω) different from those of the two signal generators (ν_m and $1/2\Omega$). Thus, filtering techniques can be used to eliminate spurious signal pick-up due to the signal generators.

For WMS detection sensitivities of 10^{-4}-10^{-5} have been demonstrated [3] and for FMS and TTFMS detector shot-noise limited performance is achievable with a sensitivity of 10^{-7}-10^{-8} [4]. Choosing a small modulation frequency involves a simpler and less expensive apparatus with somewhat easier operation. Nevertheless, the drawback is loss of sensitivity. Sensitivities possible to obtain with different FM methods are listed in Ref. [3]. Our experimental arrangements used for TTFMS, normally has a detection sensitivity around 10^{-6}. The high sensitivity is suitable for work on small volumes of the absorbing gas, and it is possible to work in the near-infrared region, where molecular transitions are weak, but inexpensive GaAs diode lasers manufactured for communication purposes are commercially available. The GaAs lasers are also simple to operate.

The early FMS measurements used dye lasers and an external electro-optic modulator, which required modulation powers of several watts to generate a sufficient modulation depth. Today, mostly diode lasers are used. These lasers can be frequency modulated conveniently by applying the ac current capacitively to the laser injection current. Many species have weak overtone and combination bands within the wavelength range of conventional GaAs diode laser technology (0.7-1.7 μm) (e.g., O_2, H_2O, CH_4, NH_3, CO, CO_2, NO, NO_2). Using PbS diode lasers in the 3-30 μm wavelength range, where most molecules have strong fundamental vibrational transitions, would allow a wide range of minor and major species in smaller samples to be probed. However, these lasers require cryogenic cooling, are expensive and not simple to operate. With the use of GaAs diode lasers and standard RF components, multi-laser arrangements for simultaneous data acquisition are conceivable.

Measurements

Figure 1 shows the basic experimental arrangement, which we use for TTFMS. The diode lasers are commercially available GaAlAs lasers from different manufacturers, and operate in the wavelength range of 750-850 nm. The lasers are temperature and current controlled by a Melles-Griot 06DLD203 precision diode laser driver. Wavelength tuning of the laser is accomplished by current ramps or current pulses. The two modulation frequencies ($\nu_m \pm 1/2\Omega$) are generated by mixing the frequencies from two different signal generators in a radio frequency mixer. Normally, we use modulation frequencies in the region of 600-900 MHz and signal demodulation at about 10 MHz. The homodyne signal amplitude is recovered by a double balanced mixer driven on the RF port by the amplified detector signal and on the LO port by the suitably phase matched and frequency doubled output Ω from the low-frequency signal generator. The demodulated absorption signal from the mixer is amplified by a low-noise preamplifier with a variable low-pass filter. The spectra is recorded on a Tektronix 2431L digital oscilloscope, connected to a 386 computer over a GPIB interface. The signal averaging is made in the computer, by adding consecutive spectra consisting of 1024 channels of data.

Water activity measurements: The water vapor concentration in a gas in chemical equilibrium with a solution depends on the water activity in the solution. By measuring the light absorption due to the water vapor over the solution relative to the absorption over a pure water reference, the water activity in the solution can be determined [5]. With laser techniques the relative water vapor concentration can be measured independently of other components present in the gas. This opens new possibilities in chemical analysis. The water activity a is related to the vapor pressure $p^{\circ}_{H_2O}$ over the pure water solvent and the vapor pressure p_{H_2O} when in a mixture through

$$a = \frac{p_{H_2O}}{p^{\circ}_{H_2O}}.$$

The water activity depends on the composition and the concentrations of the dissolved molecules in the solution, and is coupled to the interactions between the molecules [6]. The chemical potential μ, an important quantity in describing thermodynamic properties of water solutions, can be determined from the activity *a* of the water.

Figure 2 shows consecutive measurements of the TTFMS signal from a 0.5% H_2O absorption at 819 nm, when a 1M NaCl solution is replaced with the pure water reference. After correction for a small contribution from H_2O in the beam path outside the absorption cell, the H_2O pressure change in the cell is calculated to be (3.68 ± 0.30)%. The signal-to-noise ratio in Fig. 2 is estimated to be 14, which gives a minimum detectable pressure change of 0.3%, with a signal-to-noise ratio of one, with our current system. We find that the noise seen in Fig. 4 is caused by optical feedback.

Tomography: Non-intrusive spatially resolved measurements of gas concentrations are important in fluid flow, combustion and heat transfer research. By combining multi-angle absorption measurements with tomographic reconstruction, quantitative and spatially resolved measurements may be performed [7]. Due to the low absorbance of most gaseous species in the visible wavelength region, previous attempts in optical absorption tomography have been restricted to specially selected species in order to obtain sufficiently high signal-to-noise ratio for the tomographic reconstruction [8,9]. Combining tomography with TTFMS, extends the possibilities for quantitative and spatially resolved measurements to a vast number of species.

Figure 3 shows a tomographic reconstruction of the oxygen concentration in a section 3.2 mm above a nozzle orifice (4×18 mm), using a modified multiplicative algebraic reconstruction algorithm (MART) [10]. Each pixel is 0.5×0.5 mm. Six projection angles 30° apart were recorded. In each projection, 81 consecutive measurements of the TTFMS signal were made with a data acquisition time of 13 minutes. An optical dual-channel technique with balanced homodyne detection [11] was employed to suppress optical interference fringes and effectively cancel the background absorption due to the atmospheric O_2. The nozzle was translated across one of the detection channels with a step length of 0.5 mm, using a computer controlled stepping motor. The O_2 jet was flowing at 10 liters/minute from the nozzle. The expected flat-top behaviour of the laminar flow is clearly visible in the image. The average oxygen concentration on the plateau was determined to 104%, with a standard deviation of 4.7 %, using 250 waveforms in the signal averaging. The absorption measurements were performed on the R5Q6 line at λ=761.140 nm in the oxygen A-band. When transmitting the laser beam along the shortest path length through the asymmetric flow the peak absorption was 3×10^{-4} and the signal-to-noise ratio 300.

Line profile analysis: The line shape of a TTFMS signal depends strongly on the absorption linewidth, modulation frequency and the frequency modulation (FM) index. Employing the peak-to-peak value of the TTFMS signal to estimate the concentration of a species in a gas at different composition and/or pressure, leads to large uncertainties when the absorption line profile is altered. For example, in the above mentioned water activity measurements, the absorption linewidth increases due to collisional self-broadening when the water vapor pressure increases, leading to a systematic error in the relative pressure determination. Although the change of the linewidth due to the collisional self-broadening is linearly proportional to the vapor pressure, the TTFMS peak-to-peak value is not. The requirements of performing quantitative measurements

increase the importance of a method providing accurate information of the absorption line parameters out of the TTFMS spectrum. We have shown that it is possible to determine the line parameters accurately from TTFMS spectra, using a least-squares fitting procedure [12]. This widens the applicability of TTFMS in quantitative measurements using weak absorptions, and also provides a useful tool in high resolution spectroscopy, when sufficiently strong absorptions are difficult to obtain, e.g. when studying gases at high temperatures.

Figure 4 shows the oxygen R5Q6, R23Q24 and R33Q34 lines in the A-band, recorded using TTFMS with an optical absorption path length of about 0.4 m in open atmosphere, giving a peak absorption of 1.0×10^{-2}, 1.3×10^{-3}, and 4.5×10^{-5}, respectively. The lower part of Fig. 4 shows, in a greatly expanded scale, the residual errors after subtracting the experimental spectra with the fitted Voigt profile. The residual errors after the fit to the recorded spectrum of the R5Q6 line are less than ±0.3% of the signal peak-to-peak value, which indicates a good validity of the TTFMS theory and the Voigt profile employed.

The adjustable parameters in the non-linear least-squares fitting procedure were the Lorentzian contribution and the Gaussian contribution to the Voigt profile, line intensity (arbitrary scale), line position, and the amplitude modulation (AM) index. When trying to include the frequency modulation (FM) index as a variable, it was found, when the modulation frequency was smaller than the Lorentzian halfwidth, that increasing the FM index and decreasing the Lorentzian contribution (or vice versa) gave a similar result to the signal profile. Therefore, in order to achieve a higher accuracy in the line parameter determination, the Lorentzian contribution and the FM index was determined with a semi-experimental approach, using several spectra recorded with different FM index [12].

Acknowledgements

The authors would like to thank I. Harwigsson and B. Jönsson (University of Lund) and V. G. Avetisov and H. M. Hertz (Lund Institute of Technology) for collaboration in the projects. This work was supported by the Swedish Board for Industrial and Technical Development and the Swedish Research Council for Engineering Science.

References

1. G. R. Janik, C. B. Carlisle, and T. F. Gallagher, J. Opt. Soc. Am. **B3**, 1070 (1986).
2. L-G. Wang, D. A. Tate, H. Riris, and T. F. Gallagher, J. Opt. Soc. Am. **B6**, 871 (1989).
3. J. A. Silver, Appl. Opt. **31**, 707 (1992).
4. C. B. Carlisle, D. E. Cooper, and P. Preier, Appl. Opt. **28**, 2567 (1989).
5. P. Kauranen, I. Harwigsson and B. Jönsson, J. Phys. Chem. **98**, 1411 (1994).
6. J. N. Israelachvili, *Intermolecular and surface forces*; Academic Press: London, New York, 1985.
7. P. Kauranen, H. M. Hertz, and S. Svanberg, *Tomographic imaging of fluid flows using two-tone frequency-modulation spectroscopy*, Opt. Lett. (1994), in press.
8. R. J. Santoro, H. G. Semerjian, P. J. Emmerman, and R. Goulard, Int. J. Heat Mass Transfer **24**, 1139 (1981).
9. G. W. Faris and R. L. Byer, Opt. Lett. **11**, 413 (1986).
10. H. M. Hertz, Appl. Opt **25**, 914-921 (1986).
11. C. B. Carlisle and D. E. Cooper, Opt. Lett. **14**, 1306, (1989).
12. P. Kauranen, and V. G. Avetisov, Opt. Comm. **106**, 213 (1994).

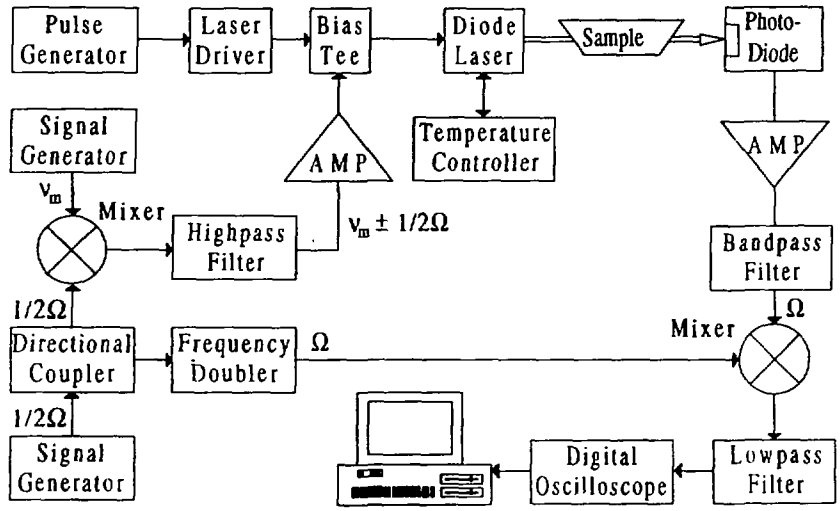

Fig. 1. Schematic diagram of a typical two-tone frequency modulation spectroscopy (TTFMS) apparatus.

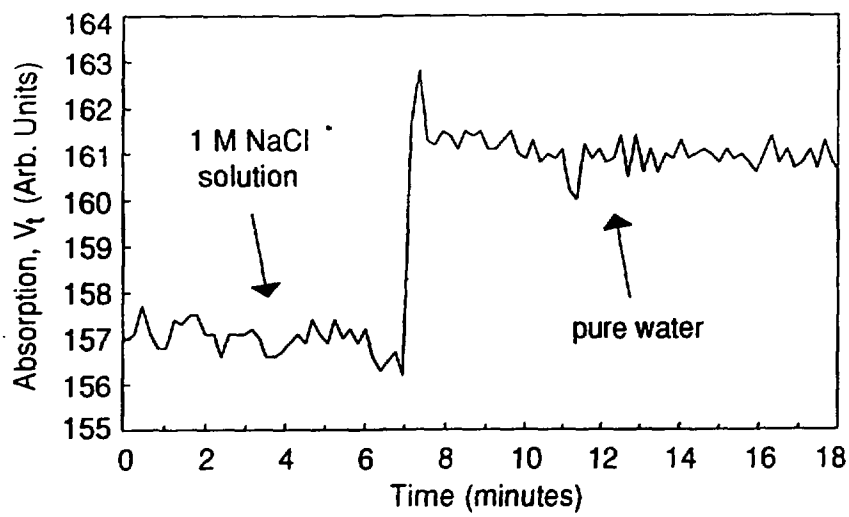

Fig. 2. Recording of the peak-to-peak value of the TTFMS signal, when a 1.0 M NaCl solution, in connection with the absorption cell, is replaced by pure water (from Ref. 5).

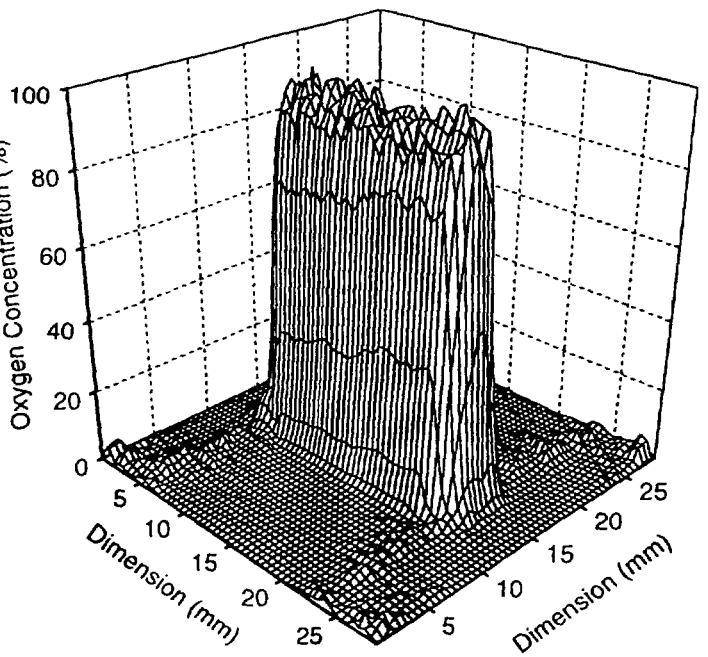

Fig. 3. Tomographic reconstruction of the concentration of O_2 in an expanding flow, 3.2 mm above a rectangular (4 × 18 mm) nozzle (from Ref. 7).

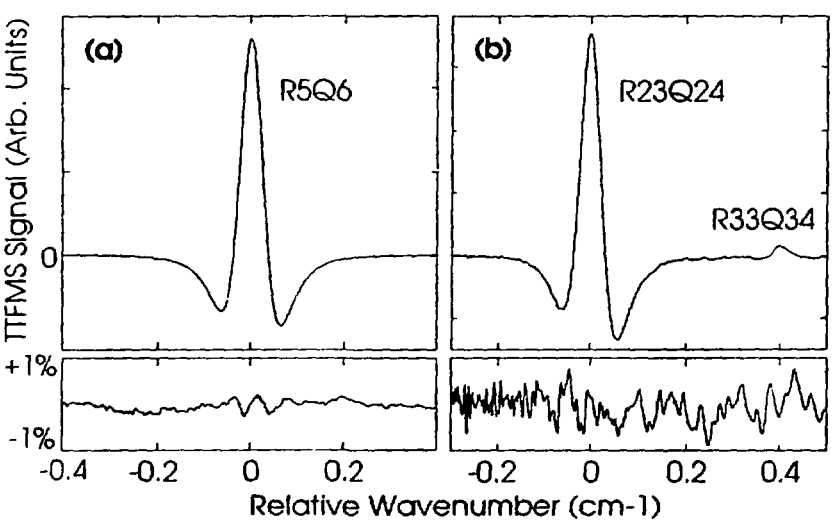

Fig. 4. Results of least-squares fittings of two-tone spectra using a Voigt profile. The upper traces show the experimental two-tone spectra. The lower traces are the residual errors, in an expanded scale (±1% of the signal peak-to-peak value), obtained from the least-squares fittings. The peak absorptions were 1.0×10^{-2}, 1.3×10^{-3}, and 4.5×10^{-5}, respectively (from Ref. 12).

Medical diagnostics using laser induced fluorescence

Peter Kauranen and Sune Svanberg
Department of Physics, Lund Institute of Technology,
P.O. Box 118, S-221 00 Lund, Sweden

Introduction

While therapeutical aspects of lasers in medicine have been very dominant, tissue diagnostics techniques using laser spectroscopic techniques are now strongly emerging. Several factors contribute to the increasing interest for laser tissue diagnostics:

- Optical monitoring is non-intrusive in nature
- Non-ionizing radiation is employed
- Real-time data representation is possible
- Spectroscopy allows molecular specificity in analysis
- Point monitoring or imaging capability can be employed
- Integration of laser diagnostics and therapy is possible.

Thus, spectroscopic techniques are providing new possibilities for tissue diagnostics. Laser-induced fluorescence spectra for biological molecules have comparatively little structure, but sometimes have sufficient specificity to allow demarcation between diseased and surrounding normal tissue. This is particularly true if tumour marking has been performed with tumour-seeking agents, such as hematoporphyrin derivative (HPD) or δ-amino levulinic acid (ALA). Also atherosclerotically transformed vessel wall can be identified providing a means for spectroscopic guidance for angioplasty. Time-integrated monitoring of the full fluorescence spectra as well as time-resolved data for chosen fluorescence wavelengths can be used to optimise the demarcation capability. By time-resolved spectroscopy it is possible to follow the transport of photons through tissue. In particular, time-resolved transillumination with detection of only the first emerging photons allows enhanced viewing through tissue by reducing the image blurring due to light multiple scattering.

Light interaction in biological tissue

Molecular Absorption of Laser Light: When tissue is irradiated by laser light, a small fraction of the light is reflected but most of it penetrates into the tissue where it is either absorbed or scattered. In certain wavelength regions absorption strongly dominates over scattering. A schematic diagram of the absorption of some important biological constituents and chromophores, such as water, proteins, nucleic acids, haemoglobin and melanin is shown in Fig. 1[1]. Haemoglobin in the blood absorbs light in a broad wavelength region up to red light (about 600 nm) with a pronounced absorption maximum at about 400 nm. Between 600 nm and 1.3 μm the attenuation coefficients of the tissue molecules are comparatively small, resulting in a wavelength region with favourable light penetration properties. Considering the total tissue absorption, it can be noted that the human body is as transparent as can be at about 1 μm.

Laser-Induced Tissue Heating: Laser-induced tissue heating occurs as a result of absorption of light by biomolecules followed by a non-radiating deexcitation. Heating leads to protein coagulation (~60°C), body fluid boiling (~100 °C) and tissue carbonisation (~200 °C)

that can be used for haemostasis and tissue surgery. This is a major application of lasers in medicine, having much impact in opthtalmology, dermatology and general surgery.

Laser-Induced Photochemistry: Optically excited molecules can, instead of releasing their excess energy as heat, transfer their energy to other molecules inducing chemical reactions of therapeutic interest. Optical treatment of psoriasis patients, or new-born infants with an excess of bilirubin, are well-known examples of medical photochemistry. Photodynamic tumour therapy (PDT) using tumour-seeking agents is a further example of special interest. The most commonly used tumour sensitiser is haematoporphyrin derivative (HPD), which is commercially available under the trade name of Photofrin. The absorption curve of HPD is included in Fig. 1. When injected intravenously such molecules are selectively retained to a higher degree in malignant tumour tissue compared to other surrounding tissue. Following light irradiation, HPD molecules become excited. The molecules can then be deexcited following two main pathways. In the first one, the molecules non-radiatively are transferred to the bottom of the first excited band, from where a radiative decay follows with the emission of a dual-peaked fluorescence light distribution in the red spectral region. This emission can be used for the diagnostics of malignant tumours, since the characteristic red fluorescence only follows from irradiated tissue that has retained the HPD molecules. In a second deexcitation pathway the molecules are transferred into the triplet state. From here the excitation energy can be transferred to ground-state tissue oxygen molecules that are excited into their singlet state. Singlet state oxygen is known to be an extremely toxic agent for living cells. As the HPD in the cells mediates this energy transfer, which results in singlet-oxygen formation, the cells are transformed from viable malignant cells to non-viable necrotic cells. This is the essence of photodynamic therapy.

The only observed side-effect of HPD is skin photosensitation 3-4 weeks following administration. This side-effect can be avoided in the case of superficial tumours by using topical application instead of systemic injection of a sensitising drug. Topically applied δ-amino levulinic acid (ALA) can be used for PDT of superficial skin tumours[2]. ALA penetrates the damaged keratin in the dermis but not the undamaged parts. ALA is a precursor in the biosynthetic pathway of the blood pigment haemoglobin. ALA is a non-photoactive substance, but within the haem cycle it is transformed into protoporphyrin, which is a photodynamically very potent agent. The conversion of ALA into protoporphyrin in tumours can be readily followed using laser-induced fluorescence[2].

Tumour detection using laser induced fluorescence

For large biomolecules the fluorescence normally exhibits a rather structure-less intensity distribution as a function of wavelength, reflecting the distribution of substates in the ground electronic level. However, by choosing the excitation wavelength properly and accurately analysing the fluorescence light distribution, it is frequently possible to obtain diagnostic information for the tissue molecules. Fig. 2[3] shows spectra for tumour as well as for surrounding normal tissue and for two excitation wavelengths, 337 and 405 nm. The sample chosen is a rat tumour in a muscle environment[4]. The rat had been injected by a dose of haematoporphyrin derivative (Photofrin) 2 days earlier. For both excitation wavelengths a broad intensity distribution extending from the blue to the near IR region is obtained.

The tumour spectra show the characteristic dual-peaked fluorescence signal from HPD in the red wavelength region. This signal is less prominent in the normal tissue due to the selective retention of the drug in tumour tissue. The signal in the blue-green region, peaking at about 470 nm, is called the autofluorescence, since it is due to the natural chromophores in the tissue. The blue-green fluorescence is much stronger and the red HPD signal much weaker when 337 nm is chosen as the excitation wavelength. This can be understood from the

absorption curves in Fig. 1. 405 nm corresponds to the absorption maximum (the Soret band) of the HPD molecules, and excitation here is more efficient than at 337 nm. An interesting observation relating to Fig. 2 is that the intensity of the blue-green signal is reduced in tumour tissue as compared to normal one. These observations form the basis for efficient tumour detection and demarcation using laser-induced fluorescence after injection of a tumour-seeking drug: the red fluorescence increases and the blue-green fluorescence decreases in a tumour. Both effects can be utilised in a convenient way by dividing the red signal intensity by the blue intensity[5]. This is illustrated in Fig. 3[6] for the case of a scan through a tumour, inoculated in a rat brain. The rat had been injected with Photofrin (1 mg/kg bodyweight) 24 hours before the animal was sacrificed and the fluorescence investigation was performed. Typical spectra for normal and tumour regions are included in the figure, with the red intensity at 630 nm denoted by A´ and the blue intensity at 470 denoted by B. The background-free HPD signal at 630 nm is denoted by A. In the scan the red increase and the blue decrease in the tumour are very evident. Contrast enhancement is obtained by forming the ratio A/B. The ratio signal is basically only sensitive to the intrinsic properties of the tissue.

The excitation source used in the recording of the data in Fig. 2 and 3, was a sealed-off nitrogen laser, emitting at 337 nm, generating typically 3 ns long pulses at 10 Hz, and with the possibility to pump a compact dye laser. The excitation laser light was focused into an optical fiber that can be sterilised when used in surgical procedures or used through the biopsy channel of an endoscope. The fluorescence light was captured through the same fiber separated from the excitation light by a dichroic mirror.

A point-tmonitoring fluorescence system has been assembled and used to evaluate its potential for early tumour diagnostics at a large number of clinical examinations (see e.g. Fig. 4)[7,8]. At several occasions lesions not found by normal visual examination have been detected.

Multi-Color Fluorescence Imaging of Tumours: It is of great diagnostic interest to extend fluorescence monitoring with incorporation of the contrast-enhancement techniques illustrated in Fig. 3 into imaging measurements. This has been accomplished in Lund, by developing a multi-color fluorescence imaging system, which provides full two-dimensional imaging[9,10,11,12]. In order to simultaneously obtain spatial and spectral resolution, the fluorescence light is divided using a multi-mirror arrangement as illustrated in Fig. 5. By using a spherical mirror which is divided into four individually adjustable sectors, four identical images can be sent to an intensified matrix detector, a CCD camera. By placing optical filters in front off the different mirror sectors, fluorescence images in selected colors are obtained simultaneously. In the four different images computerised calculations of dimensionless function values can be performed for each spatial location of the tissue investigated and a generalised image in an optimised contrast function can be produced. This function would normally be the ratio between the background-free 630 nm peak intensity A and the blue-green intensity B at about 470 nm. A properly weighted recording at 600 nm (kD) provides the background intensity. The weighting factor k also takes differences in optical efficiency into account and is adjusted to result in a zero intensity value for A= (A´-kD) when no tumour is present. This system can be used together with endoscopes of different types allowing, e.g. lung and bladder investigations.

Fluorescence images at 630, 600 and 470 nm are shown in Fig. 6[12] for a human T-cell lymphoma tumour. Also included is the resulting image using the contrast function (A´-kD)/B, showing the tumour with a very clear demarcation towards surrounding normal tissue. A nitrogen-laser-pumped dye laser was employed for fluorescence excitation.

Time-Resolved Monitoring: Using short-pulse excitation, it is also possible to measure the decay time for the fluorescence light yielding additional information for tissue characterisation, e.g. for distinguishing atherosclerotically diseased vessel wall from normal vessel wall[13,14]. The fluorescence from the diseased region has a longer decay time compared

to the normal vessel wall tissue. By a detailed analysis it is possible to unfold the decay into three components with different decay times[13]. This can be utilised for assessing the tissue in front of the fibre tip. The intensity of "late" fluorescence (5-15 ns) can be divided by the intensity of "early" (0-5 ns) fluorescence to produce a signal that is higher for plaque than for normal vessel wall. Such a signal can be used to control the firing of the high-energy laser used for plaque removal.

Optical transillumination of tissue

Time-resolved transillumination allows enhanced wieving through tissue. X-ray diagnostic techniques are the conventional means for such imaging that has been brought to a very high level of sophistication. However, ionising radiation is accompanied by a certain risk of mutagenicity[15]. It would be very desirable to use optical radiation for transillumination of tissue to avoid this risk and also to allow spectroscopic recordings of molecular-specific absorption. Red light penetrates tissue quite well. The reason is the quickly decreasing absorption of haemoglobin beyond 600 nm. The low intensity of the transmitted light through thick tissue is not a problem, since very sensitive light detectors exist, but rather the strong multiple scattering from the cell structures, washing out all the spatial information. Recently, a lot of research has been initiated to overcome these problems[16,17], e.g. by using time-resolved photon-counting techniques employing picosecond red laser pulses[18,19,20]. Because of the multiple scattering, most of the photons penetrating the tissue have spent a long time in the tissue, while only very few photons arrive to the detector at the nominal propagation time without disruptions. However, by selecting a very small detection time window and recording the very first photons, it is possible to look at just the "fastest" photons coming out of the tissue. If an obstacle, such as a bone or a tumour blocks the passage, a shadow will be created for the selected subgroup of very early photons. For thicker samples there are no unscattered photons. Still, the first photons have been minimally scattered producing a more clear image. The principle is shown in Fig. 7. By scanning the tissue under investigation, a transillumination image can be created. Recently we have shown, that such measurement can be performed using a pulsed diode-laser source, operating at 815 nm and producing 30 ps long pulses at a repetition rate of 10 MHz, making the technique very realistic[20]. Images of a ductal breast carcinoma in a newly resected breast are given in Fig. 8. In the time-integrated light the tumour cannot be seen. It was also difficult to detect using conventional X-ray mammography.

Acknowledgements

The authors gratefully acknowledge stimulating collaboration with a large number of collegues within the Lund University Medical Laser Center. This work was supported by the Swedish Research Council for Engineering Sciences, The Swedish Board for Technical and Industrial Development, the Swedish Cancer Foundation and the Swedish Medical Research Council.

References

1. J.-L. Boulnois, Photophysical processes in laser-tissue interactions, in Laser Applications in Cardiovascular Diseases, (R. Ginsberg, ed.), Futura, New York (1987).
2. K. Svanberg, T. Andersson, D. Killander, C. Stenram, S. Andersson-Engels, R. Berg, J. Johansson, and S. Svanberg, *Photodynamic therapy of non-melanoma cancers of the skin utilizing topical δ-amino levulinic acid application and laser irradiation*, Submitted to Brit. J. of Dermatology.
3. S. Andersson-Engels, J. Ankerst, S. Montán, K. Svanberg and S. Svanberg, Lasers Med. Sci. 3, 239 (1988).
4. G. Hedlund and H.O. Sjögren, Int. J. Cancer 26, 1-73 (1980).
5. J. Ankerst, S. Montán, K. Svanberg and S. Svanberg, Applied Spectroscopy 38, 890 (1984).

6. S. Andersson-Engels, A. Brun, E. Kjellén, S. Montán, L. G. Salford, L-G. Strömblad, K. Svanberg and S. Svanberg, Lasers in Med. Sci. 4, 241 (1989).
7. S. Andersson-Engels, Å. Elner, J. Johansson, S-E. Karlsson, L. G. Salford, L-G. Strömblad, K. Svanberg and S. Svanberg, Lasers in Med. Sci. 6, 415-424 (1991).
8. K. Svanberg, S. Andersson-Engels, L. Baert, E. Bak-Jensen, R. Berg, A. Brun, S. Colleen, I. Idvall, M-A. D'Hallewin, C. Ingvar, J. Johansson, S-E. Karlsson, R. Lundgren, L. G. Salford, U. Stenram, L-G. Strömblad, S. Svanberg, I. Wang, *Tissue characterization in some clinical specialities utilizing laser-induced fluorescence*, Proc. SPIE 2135:1 (1994).
9. P. S. Andersson, S. Montán and S. Svanberg, IEEE J Quant. Electr. 23, 1798 (1987).
10. S. Andersson-Engels, J. Johansson, and S. Svanberg, Multicolor fluorescence imaging system for fluorescence diagnostics, SPIE Vol. 1205, 179-189, Bellingham (1990).
11. S. Andersson-Engels, J. Johansson and S. Svanberg, *Medical diagnostics system based on simultaneous multi-spectral fluorescence imaging*, Appl. Opt., accepted (1994).
12. S. Andersson-Engels, R. Berg, K. Svanberg and S. Svanberg, *Multi-colour fluorescence imaging in combination with photodynamic therapy of δ -amino levalinic acid (ALA) sensitised skin malignancies*, to appear.
13. S. Andersson-Engels, J. Johansson and S. Svanberg, Spectrochima Acta 46A, 1203 (1990).
14. O. S. Wolfbeis (ed.), Fluorescence Spectroscopy; New Methods and Applications, Springer, Heidelberg (1992).
15. M. Swift, D. Morrell, R. M. Massey and C. L. Chase, New Engl. J. Med. 325, 1831 (1991).
16. B. Chance, ed., Photon Migration in Tissue, Plenum, New York (1989).
17. B. Chance and G. Müller (eds), Optical Tomography, SPIE, Bellingham (1993).
18. S. Andersson-Engels, R. Berg, S. Svanberg and O. Jarlman, Opt. Letters 15, 1179 (1990).
19. S. Andersson-Engels, R. Berg and S. Svanberg, J. Photochem. Photobiol. 16, 155-167 (1992).
20. R. Berg, O. Jarlman and S. Svanberg, Appl. Opt. 32, 574-579 (1993).

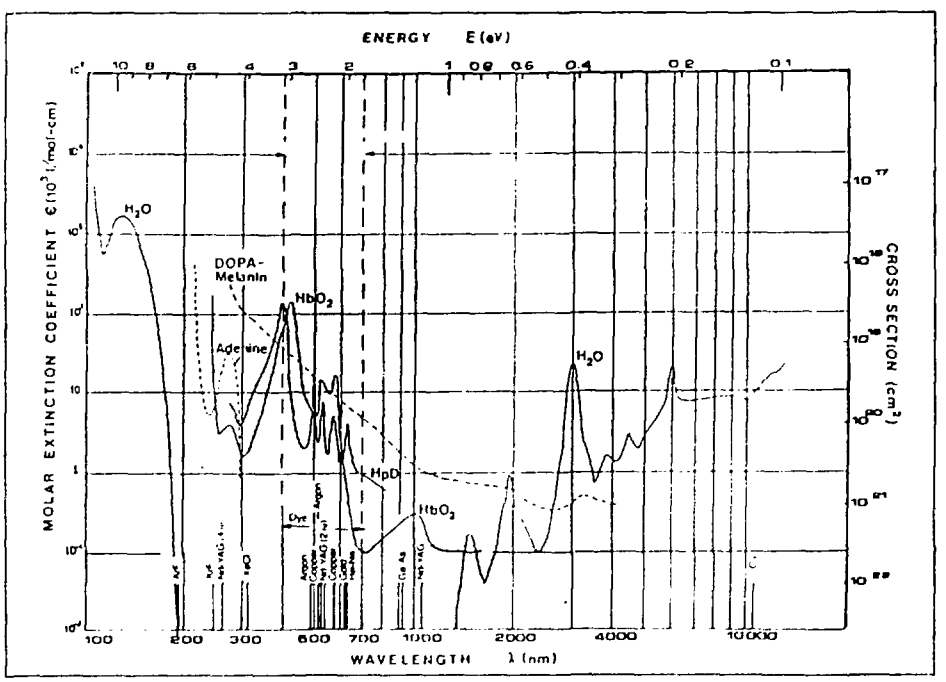

Fig. 1. Absorption properties of biological molecules: water, haemoglobin, melanin, haematoporphyrin derivative (HPD) and adenine (From Ref. 1).

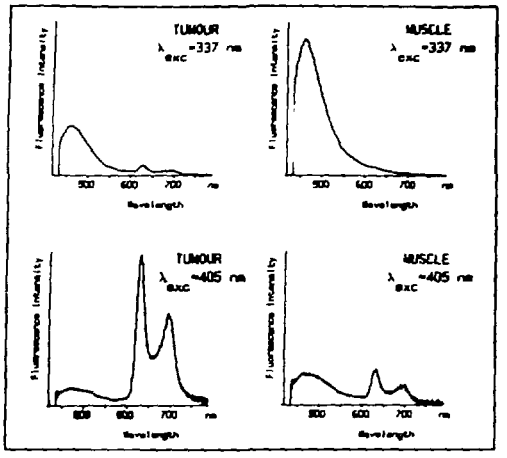

Fig. 2. Laser-induced fluorescence spectra for an experimental tumor (a human colon adenocarcinoma inoculated in rat muscle), and normal surrounding tissue. The rat had been injected with a dose of haematoporphyrin derivative about 2 days before the investigation. Two excitation wavelengths, 337 and 405 nm, are chosen to illustrate the influence of the wavelength choice.

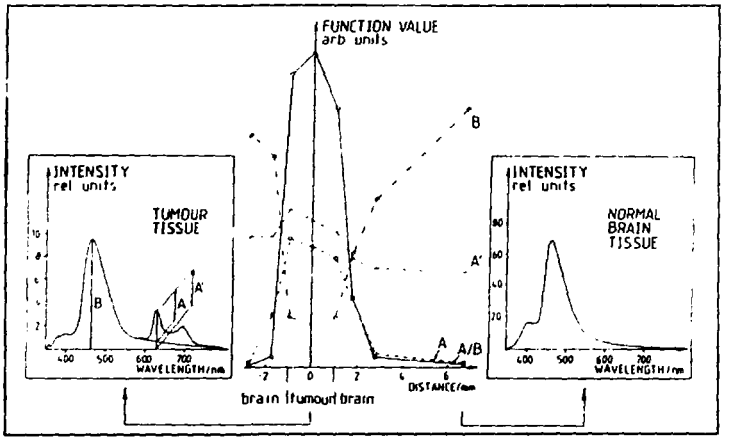

Fig. 3. Fluorescence data obtained in a scan across an experimental glioma (TCVC) in a rat injected with 1 mg/kg b.w. Photofrin 24 hours earlier. Laser-induced fluorescence spectra of tumor tissue and surrounding normal brain parenchyma are also shown. The background-free HPD-related signal is denoted A, while the total signal at 630 nm is denoted A' and the autofluorescence B. The dimensionless ratio A/B shows a strong contrast enhancement (From Ref. 6).

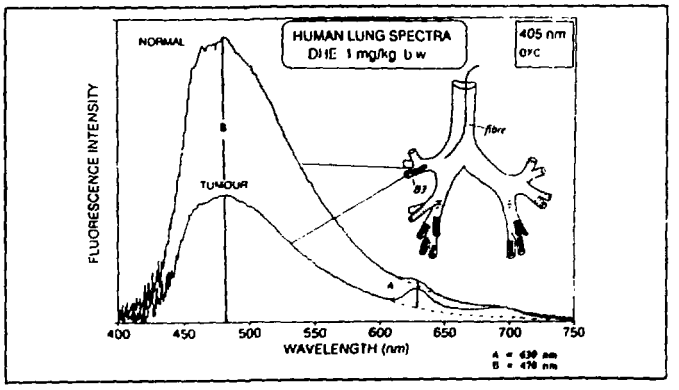

Fig. 4. Fluorescence spectra for a bronchial carcinoma and adjacent normal mucosa in a patient that had received a dose of Photofrin at a concentration of 1 mg/kg bodyweight 48 hours before the fluorescence investigation.

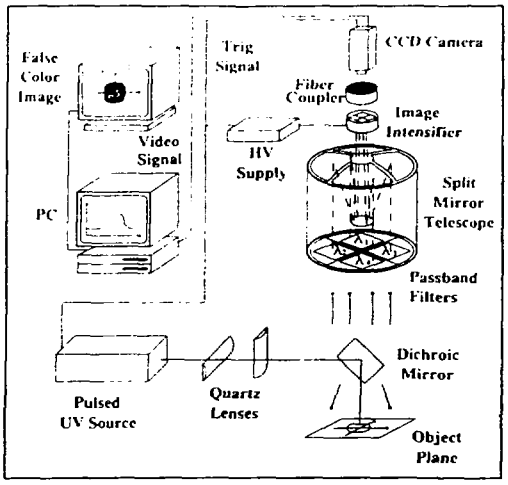

Fig. 5. Diagram showing the basic construction of a multi-color fluorescence imaging system (From Ref. 10).

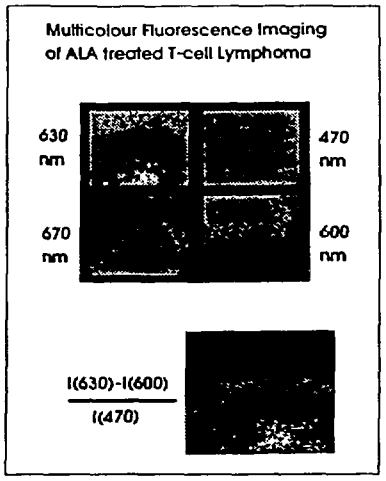

Fig. 6. Imaging fluorescence recordings of a human T-cell lymphoma tumor in a patient that had been subject to topical ALA application 6 hours before the investigation. Individual images at 630, 600 and 470 nm are shown together with a processed image using the data in the three individual images (From Ref. 12).

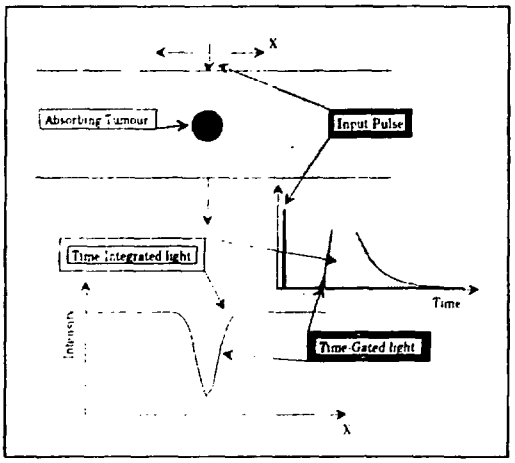

Fig 7. Gated viewing through tissue. An enhanced spatial resolution is obtained by selecting "early" light only (From Ref. 17).

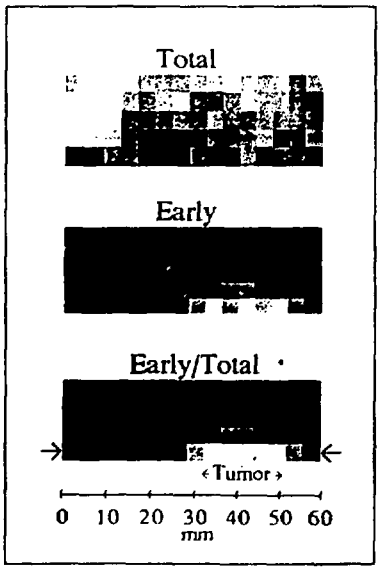

Fig. 8. Two-dimensional transillumination scans through a resected breast sample containing a ductal carcinoma. The tumour clearly emerges in the early

Monitoring of atmospheric pollutant and vegetation status using laser radar

Peter Kauranen and Sune Svanberg
Department of Physics, Lund Institute of Technology,
P.O. Box 118, S-221 00 Lund, Sweden

Introduction

Advanced techniques are needed to monitor our threatened environment, to evaluate pollution levels and developmental trends. Tropospheric pollution has obvious manifestations in terms of health problems, water and soil acidification, and forest damage. Human-induced stratospheric changes in the ozone layer, as evidenced by the occurrence of "ozone holes" at the polar caps, may have much more far-reaching consequences [1,2]. The "green-house" effect, due to a global increase in IR absorbing gases such as CO_2, CH_4 and N_2O is another process of paramount importance [3,4,5]. Gaseous pollutants injected into the atmosphere enter very complex atmospheric chemistry chains [1,2,6]. Laser spectroscopy provides powerful means for remote sensing of molecules in the atmosphere, yielding information on pollution levels as well as meteorological conditions. There are two mayor kinds of laser methods applicable in remote sensing [7,8]: long-path absorption monitoring, and LIDAR (Light Detection And Ranging).

Long-path absorption techniques: Using well-collimated normal light beams or laser beams it is possible to use a pathlength of several km. A single-ended arrangement can be accomplished using a corner cube retroreflector at the end of the light path and collecting the back-reflected light with a telescope. Since all detected photons have travelled the same path no range resolution is obtained and only average concentrations can be determined. Tunable diode lasers and CW line-tunable CO_2 lasers are useful coherent light sources. A powerful non-laser counterpart in DOAS (differential optical absorption spectroscopy) [9], where a distant high-pressure xenon lamp is used in combination with fast spectral scanning detection to overcome limitations posed by atmospheric scintillation.

Lidar: A laser pulse is transmitted into the atmosphere and backscattered radiation is detected as a function of time by an optical receiver, in a radar-like fashion. We will deal with two different approaches of the lidar technique: differential absorption lidar (DIAL) and fluorescence lidar.

Mie back-scattering from particles provides strong signals allowing mapping of the relative distribution of particles over large areas if the laser beam is swept [10]. Since Mie scattering theory [11,12] involves many normally inaccessible particle parameters, quantitative results are difficult to obtain. However, Mie scattering is extremely useful in providing the "distributed mirror" needed in DIAL. The principle for DIAL is schematically represented in Fig. 1 [13]. Laser light is alternatingly transmitted at a wavelength where the species under investigation absorbs, and at a neighbouring, off-resonant wavelength. In the presence of an absorbing gas cloud, the on-resonance laser intensity is attenuated passing through the cloud while the off-resonance is not. By dividing the two lidar signals by each other, most troublesome and unknown parameters are eliminated and the gas concentration as a function of the range along the beam evaluated.

Using UV pulses from the lidar transmitter, solid targets or water can be irradiated to induce fluorescence. The signal received by the lidar telescope is wavelength dispersed in a

spectrometer and is recorded with an intensified diode array detector, allowing the detection of the whole fluorescence spectrum for each laser shot. A fluorescence lidar system can be quite interesting for monitoring vegetation fluorescence and water pollutants.

Lidar system description

Figure 2 shows a mobile lidar system constructed at the Lund Institute of Technology for research and operational measurements of various species [13]. The laser, telescope and all electronics are contained in a Volvo F610 truck with a specially designed cargo compartment of size 6.0×2.3×2.1 m^3. The truck is equipped with four sturdy supporting legs that can be hydraulically lowered, achieving high stability during measurements that requires high directional accuracy in the optical system. The laser transmitter is a Nd:YAG pumped dye laser with possibility of frequency doubling and/or mixing to the UV and IR regions. The dye laser is equipped with a dual wavelength option, enabling the laser to be alternatingly fired at two different preset wavelengths. The dye laser wavelength scale can be calibrated against known spectral lines, observed with the optogalvanic signal from a hollow-cathode lamp, illuminated with a small part of the laser beam, or using the absorption in a reference cell filled with the gas to be monitored.

The outgoing laser beam is directed coaxially with a vertically mounted telescope and transmitted into the atmosphere via a large flat mirror in a retractable transmitting/receiving dome on the roof. A quartz window seals off the dome. Stepping motors are used to turn the dome and to tilt the mirror, making a measurement direction of 360 degrees horizontally and of 45 degrees vertically possible. In order to protect the mirror coating, the exiting laser beam is expanded with a ×6 beam expander. Servo motors and micrometer screws offer remote control of the final turning prism, through which the overlap between the laser transmission lobe and the telescope field of view is controlled. Two video cameras are used to control and supervise the measurement direction. A computer-controlled mechanical chopper is used to automatically block the beam during a lidar measurement in order to obtain the signal due to background light and preamplifier offset.

An adjustable field stop is placed in the focus of the receiving Newtonian telescope, by means of which the field of view can be varied from 2 to 5 mrad. After passing through an interference filter the light is detected by a photomultiplier tube. Due to the fact that the beam is emitted coaxially with the telescope, the near field backscattered light is very strong. To prevent detector overload and to reduce the dynamic range of the signal, the gain of the PMT is modulated. This is performed by changing the voltage difference in the dynode chain. The gain is very low in the beginning and does not reach its full value until 2-10 μs later (the rise time is variable).

The signal from the PMT is preamplified and captured with an 8-bit 100-MHz transient digitiser. Normally 2000 channels, each 10 ns wide, are recorded, corresponding to a lidar measuring range of 3 km. After the recording, the data are transferred by a GPIB interface to the computer where they are added into a 32-bit data array at a repetition rate of 20 Hz. A DIAL measurement cycle consists of 8 shots on each wavelength, fired alternately, and finally two shots with the chopper closed. Several cycles are then averaged and stored on disk after background subtraction. During a measurement normally 100 to 200 cycles are averaged, corresponding to a measurement time of 1.5 to 3 minutes. When vertical or horizontal scannings were performed the measurement time for each direction can be divided in several repetitions.

While system control and on-line data handling are controlled by the system computer, data processing and evaluation can be performed on a separate computer. A typical evaluation consists of three phases. First a Gaussian smoothing function of a few channels

width is applied on the raw lidar signals. Then the ratio of the lidar signal at the different wavelengths is calculated. A running average function of adjustable width is finally used to evaluate the concentration as a function of distance. Data from horizontal or vertical scans are presented as a 2D-plot with the concentration value indicated with a grey scale. The data from a vertical scan can also be transferred to a single vertical or horizontal profile with a vertical/horizontal projection.

Measurements

Numerous field measurements have been performed with the mobile lidar system for monitoring of gases like SO_2, NO_2, NO and O_3. An example of SO_2 emission measurements is shown in Fig. 3, which displays a mapping of the SO_2 distribution in a cross section of a plume downwind from a paper mill [13]. The integrated concentration over the plume cross section area multiplied with the wind velocity normal to the scan gives the total flux. In the example given in Fig. 3 the total flux was evaluated to 230 kg/h of SO_2. In these measurements also the diffuse emissions could be captured and evaluated to a SO_2 flux of 16 kg/h.

Recently, a differential absorption lidar technique for measurements of mercury down to the background concentration of about 2 ng/m^3 has been demonstrated [14]. Mercury, the only atmospheric pollution gas occurring as free atoms, is released from chlorine-alkali and coal-fired power plants, refuse incineration plants and from crematories. Mineralizations, geothermal reservoirs and volcanism are also known to be associated with elevated atomic mercury concentrations. Mercury constitutes a considerable environmental problem that has received considerable attention. It has also been suggested that geothermal energy and ore deposits might be located by focusing on associated atmospheric mercury anomalies.

An example of an atomic mercury concentration map is shown in Fig. 4. A horizontal scan above a chlorine-alkali plant is shown and the total flux was found to be 30 g/h of atomic Hg vapor by employing a vertical scan [14]. Measurements at another chlorine-alkali plant gave the total flux of 43 g/h [15]. In Fig. 5 the distribution of Hg near the cooling towers of a geothermal power plant (30 MW) is shown; Hg concentrations are given in ng/m^3 [16]. The figure is made from horizontal and vertical scans as indicated by the dots. It is interesting to see that the main part of the atomic mercury does not emerge from the top of the cooling tower but rather from the lower part. Fig. 6 shows the vertical scan of another geothermal power plant (20 MW) [16]. The total flux from this plant was evaluated to 20 g/h of atomic mercury. Very high concentrations of Hg were also found at an abandoned mercury mine [17]. The mining operations were halted in 1980 and plans to restore the area has been presented. The lidar technique can be used to localise "hot spots" to optimise sanitation. Fig. 7 shows the distribution of Hg over the central parts of the mining area. The plant for distillation of the cinnabar (HgS) ore and the smoke stacks were found to be strong sources of Hg to the atmosphere. Also the roasted cinnabar deposits contributed substantially to the local atmospheric concentration. The atomic mercury measurements were supported with gold trap point monitors and the agreement between the two methods was very good [18].

Measurement scenarios for fluorescence lidar monitoring of water and land vegetation are shown in Fig. 8 with examples of remotely recorded spectra. Algal fluorescence monitoring can be important for measuring the total marine productivity, which originates in the conversion of solar energy, CO_2 and nutrients into organic matter by microscopic phytoplankton. Recently, huge algal blooms, for instance of *Chrysochromulina polylepis*, leading to devastating consequences for most other marine life forms have occurred due to eutrophication of coastal waters. Some classes of algae exhibit LIF spectra with certain characteristic features [19] in addition to the dominating peak at 685 nm due to chlorophyll a. A blue-green

fluorescence is normally observed for water also in the absence of oil spills. This fluorescence is due to organic material (*"Gelbstoff"*).

In aquatic monitoring a strong Raman signal due to the water molecules is observed at a Raman shift of about 3400 cm^{-1} (O-H stretch vibration) seen at ~403 nm in Fig. 8.a. This signal is very useful since it is possible to use as a reference to normalise algal and Gelbstoff signals to the same effective water measuring volume. A careful analysis of the shape of the water Raman signal provides information on the water temperature. Water molecules form aggregates of different sizes with slightly different Raman shifts. The relative occurrence of mono-, di-, and poly-water is temperature dependent [20,21]

Land vegetation monitoring by fluorescence lidar is shown in Fig. 8b illustrating different signatures for green and lighily yellow maple leaves. The ratio of the two chlorophyll peaks at 690 and 735 nm relates to different plant physiological conditions [22]. Land vegetation can be efficiently characterised by multispectral reflectance measurements using space-borne sensors in satellites such as LANDSAT, SPOT and ERS-1 [23]. An active remote sensing technique such as LIF might, in certain circumstances, complement passive reflectance monitoring.

Conclusions

As demonstrated by the examples chosen, the differential-absorption lidar method is a powerful technique for mapping of important atmospheric pollutants. Fluorescence lidar techniques can complement passive spaceborne sensors in studies of water pollutants and vegetation status.

Acknowledgements

The authors gratefully acknowledge fruitful co-operation with a large number of co-workers in the field of environmental remote sensing. This work was supported by the Swedish Board for Space Activities, the National Swedish Environment Protection Board, the Swedish Natural Science Research Council, and the Swedish Space Corporation.

References

1. J. H. Seinfeld, Atmospheric Chemistry and Physics of Air Pollution, Wiley, New York (1986).
2. R. P. Wayne, Chemistry of Atmospheres, Clarendon Press, Oxford (1985).
3. W. Bach, J. Pankrath and W. Kellogg, Man's Impact on Climate, Elsevier, Amsterdam eds. (1979).
4. R. Revelle, Carbon Dioxide and World Climate, Sci. Amer. 247, 33 (1982).
5. B. J. Mason, The Greenhouse Effect, Contemp. Phys. 30, 417-432 (1989).
6. B. A. Trush, The Chemistry of the Stratosphere, Rep. Prog. Phys. 51, 1341-1371 (1988).
7. R. M. Measures, Laser Remote Sensing: Fundamentals and Applications, Wiley, New York (1984).
8. D. A. Killinger, and A. Mooradian, Optical and Laser Remote Sensing, Springer Series in Optical Sciences, Vol 39, Springer-Verlag, Heidelberg, eds. (1983)
9. H. Edner, A. Sunesson, S. Svanberg, L. Uneus and S. Wallin, Appl. Opt. 25, 403 (1986).
10. H. Shimizu, Y. Sasano, H. Nakane, N. Sugimoto, I. Matsui and N. Takeuchi Appl. Opt. 24, 617 (1985).
11. H. C. Van de Hulst, Light Scattering by Small Particles, Wiley, New York (1957).
12. M. Kerker, "The Scattering of Light," Academic Press, New York (1969).
13. H. Edner, K. Fredriksson, A. Sunesson, S. Svanberg, L. Uneus and W. Wendt, Appl. Opt. 26, 4330 (1987).
14. H. Edner, G. W. Faris, A. Sunesson and S. Svanberg, Appl. Opt. 28, 921 (1989)

15. R. Ferrara, B. E. Maserti, H. Edner, P. Ragnarson, S. Svanberg and E. Wallinder, Atm. Env., 26A, 1253 (1992).
16. H. Edner, P. Ragnarson, S. Svanberg, E. Wallinder, A. DeLiso, R. Ferrara and B. E. Maserti, J. Geophys. Res., 97, 3779 (1992).
17. H. Edner, P. Ragnarson, S. Svanberg, E. Wallinder, R. Ferrara, B. E. Maserti and R. Bargagli, Sci. Total Env., 133, 1 (1993).
18. R. Ferrara, B. E. Maserti, H. Edner, P. Ragnarson, S. Svanberg and E. Wallinder, " Atmospheric mercury determinations by lidar and point monitors in environmental studies," Metal Compounds, Environment and Life, 4 eds. E. Merian and W. Haerdi (Science and Technology Letters, UK, 1992).
19. L. Celander, K. Fredriksson, B. Galle, and S. Svanberg "Investigation of Laser-Induced Fluorescence with Applications to Remote Sensing of Environmental Parameters". Göteborg Institute of Physics Reports GIPR-149, CTH, Göteborg (1978).
20. D. A. Leonard, B. Caputo, and F. E. Hoge, Appl. Opt. 18, 1732 (1979).
21. B. G. Breschi, G. Cecchi, L. Pantani, V. Raimondi, D. Tirelli, G. Valmori, P. Mazzinghi and M. Zoppi, EARSeL Adv. Rem. Sens. 1, 131-134 (1992).
22. H. K. Lichtenthaler and U. Rinderle, CRC Crit. Rev. Anal. Chem. 19, Suppl. 1, S29-S88. (1988).
23. H. S. Chen, "Space Remote Sensing Systems," Academic, Orlando (1985).
24. H. Edner, J. Johansson, S. Svanberg, E. Wallinder, G. Cecchi and L. Pantani, EARSeL Adv. Rem. Sens. 1, 42 (1992).
25. H. Edner, J. Johansson, S. Svanberg, E. Wallinder, M. Bazzani, B. Breschi, G. Cecchi, L. Pantani, B. Radicati, V. Raimondi, D. Tirelli and G. Valmori, EARSeL Adv. Rem. Sens. 1, 119 (1992).

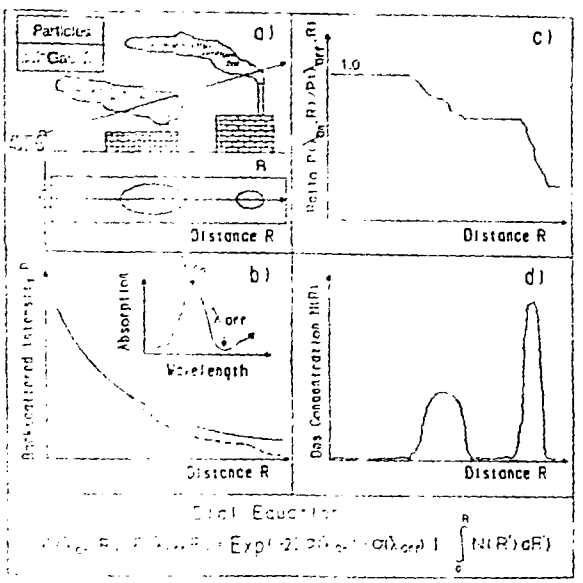

Fig. 1. The principal of the differential absorption lidar (DIAL) measurements: (a) pollution measurement situation, (b) back-scattered laser intensity for the on- and off-resonance wavelengths, (c) ratio (DIAL) curve, (d) evaluated gas concentration (From Ref. 13).

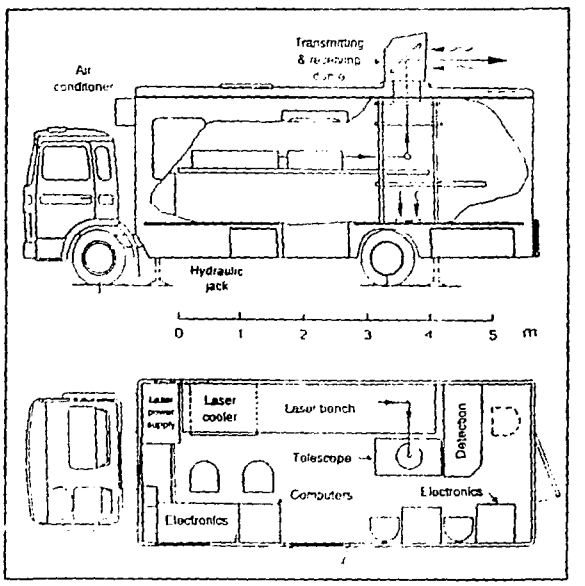

Fig. 2. Overview of the mobile DIAL system (From Ref. 13).

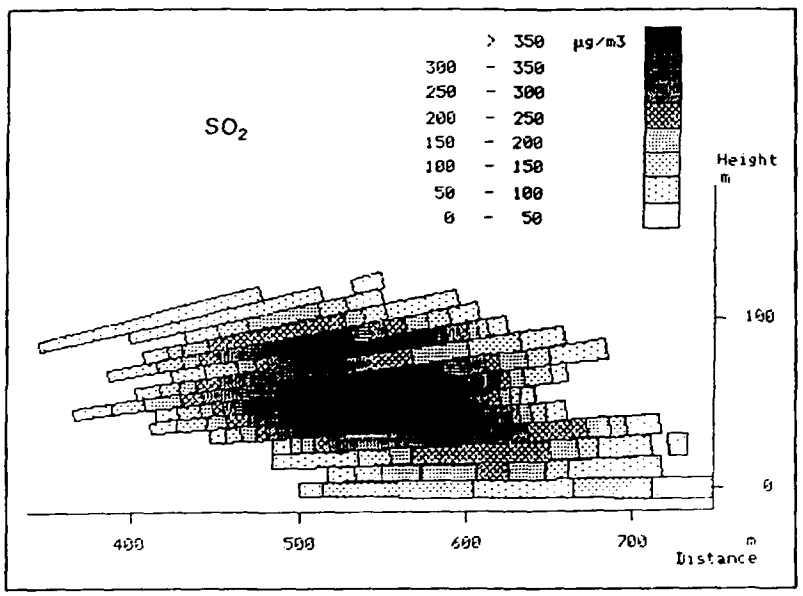

Fig. 3. Mapping of a cross section of an SO_2 plume from a papermill (From Ref. 13).

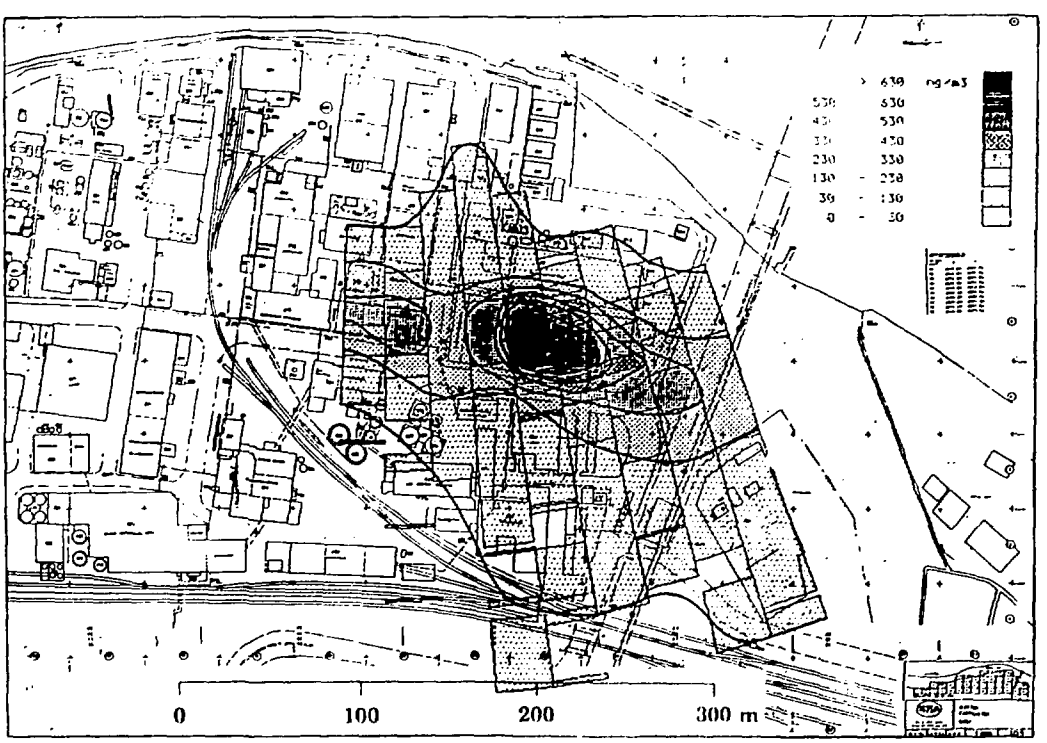

Fig. 4. Mapping of the Hg distribution over a chlorine-alkali plant (From Ref. 14).

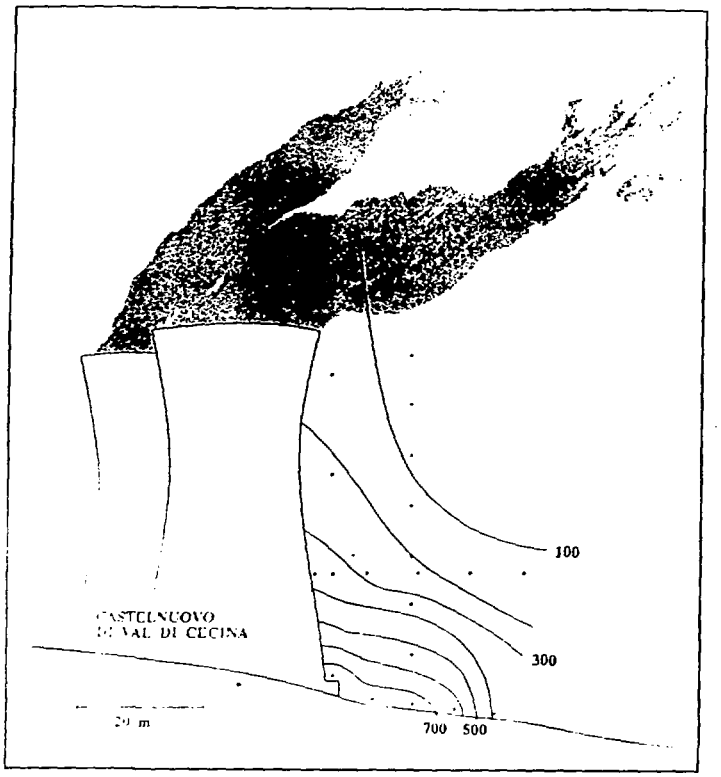

Fig. 5. Hg mapping close to the cooling towers at a geothermal power plant. Hg concentrations in ng/m^3 (From Ref. 16).

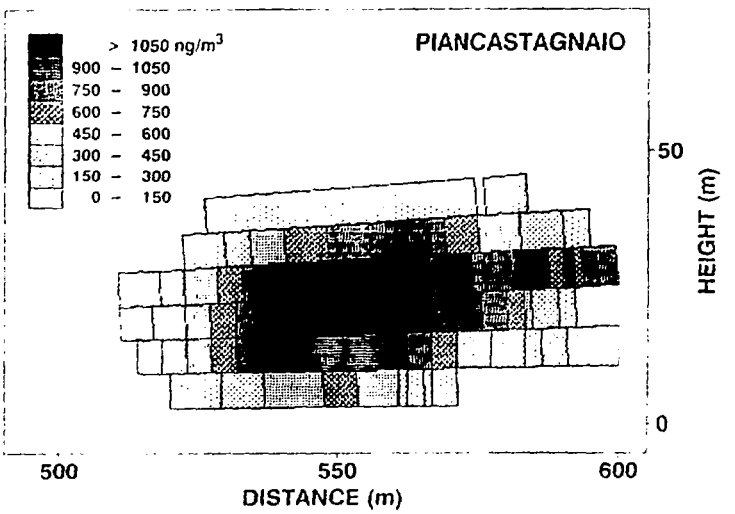

Fig. 6. Vertical scan of the Hg plume downwind a geothermal power plant (From Ref. 16).

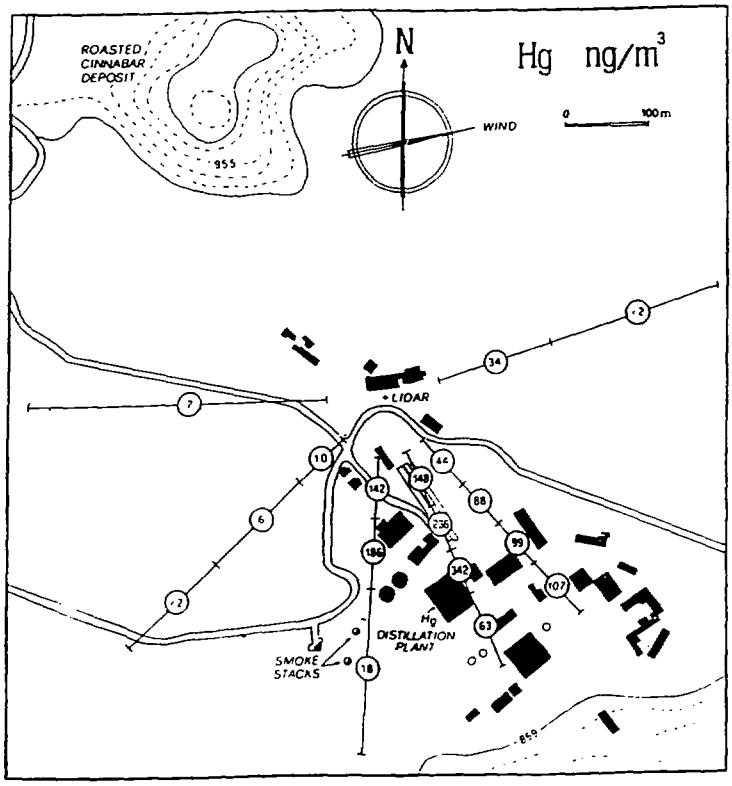

Fig. 7. Hg distribution over the central parts of an Hg mining area (From Ref. 17).

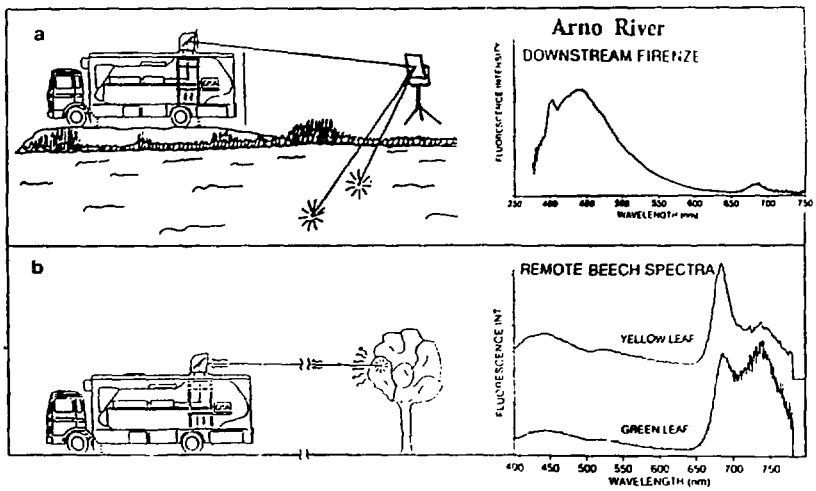

Fig. 8. Fluorescence lidar measurements of a) water (From Ref. 24) and b) terrestrial vegetation (From Ref. 25). A frequency tripled Nd:YAG laser operating at 355 nm was used. Remote laser-induced fluorescence spectra are shown for a measurement distance of about 50 m.

HIGHER ORDER CHROMATIC ABERRATION: APOCHROMATISM AND THE CHROMATIC VARIATION OF MONOCHROMATIC ABERRATIONS

J.Maxwell
Applied Optics Section
Imperial College, London

Abstract

The correction of higher order chromatic aberrations in high performance wide spectral band optical systems is the main barrier to achieving improved performance. These higher order chromatic aberrations appear in the form of longitudinal secondary spectrum, transverse secondary spectrum and chromatic variations of the monochromatic aberrations. The origins of some of the chromatic variation aberrations are discussed and some analysis methods for these aberrations are reviewed, with some suggestions for simple extensions to the methods that can be used for their calculation.

Introduction

Reflecting optical systems do not suffer from chromatic aberrations of any order, the intrinsic aberration contribution from reflecting surfaces are less than for most refracting surfaces, due to the high effective refractive index, and they are also compact and have light weight, so why use refracting optical systems at all ?

First of all, most reflecting optical systems only consist of two optical surfaces (a primary and a secondary mirror) so, in terms of the available design variables they are very simple systems, with only the same level of complexity as a thick single lens. Thus they usually have to be aspherised to achieve good aberration correction even over only small fields of view.

Secondly, most reflecting optical systems have a central obstruction, which supresses image modulation at intermediate spatial frequencies.

Last but not least, the engineering difficulties associated with reflecting and catadioptric systems, which arise from intrinsically tight tolerances and from the difficulties that the change the in focal power with bending that mirrors exhibit, usually lead to high overall project cost and high project risk.

So we frequently choose refracting optical systems in preference to reflecting or catadioptric systems. High performance refracting optical systems usually have their performance limited by higher order chromatic aberrations and it is these errors that we have to reduce if we are to achieve higher levels of performance.

These higher order chromatic errors fall into two categories: secondary spectrum effects and chromatic variations of the monochromatic aberrations; it is the latter category that is the main subject of this paper.

The correction of higher order chromatic aberrations in the form of secondary spectrum effects and particularly chromatic variation effects is not well served by the current generation of lens design software. Any lens designer who has worked on wide spectral band optical systems which require the correction of chromatic variation aberrations knows about this. The gear ratio between these errors and the changes in construction that are necessary to correct them seems to be particularly high and it is frequently the case that one has to apply what I call the method of managerial exhaustion to the problem; that is, one has to spend many more hours investigating the solution space than one's management can tolerate.

The supression of secondary spectrum effects by the choice of suitable glass types is the subject of a rich and ingenious literature (see Ref. [1] as a good example), although longitudinal effects have tended to have had much more attention than transverse effects, and what is more to the point, glass choice issues have tended to dominate the discussion, with particular emphasis on secondary spectrum, which can be conveniently illustrated with paraxially determined focal excursion curves, but which does not reveal the chromatic variation problem.

An important perspective here is that the correction of secondary spectrum in both its longitudinal and transverse manifestations is a necessary condition for the improvement of high performance refractive optical systems, but it is not a sufficient condition. Kingslake gives us an accessible and appropriate example of the problem of chromatic variation aberrations in an apochromatic system [2], where in the case he considers the best-balanced chromatic variation aberrations of an apochromatic system more or less annul any advantages that the supression of the secondary spectrum has bestowed.

Secondary spectrum effects

Conventional refracting optical systems, which use glasses with different dispersions to correct chromatic aberration by balancing large opposing focal powers, suffer from secondary spectrum effects, such that when two wavelengths at the end of the working spectral band are made to focus together the wavelengths in between focus elsewhere. The effect shows itself longitudinally as a defect of focus of the order of 1/2000 of the focal length. If we choose the usual 546, 656 and 435nm design wavelengths for the visual waveband this error can be reduced by the use of special glasses and or by the combination of several different types of glass, and this is particularly necessary in complex systems where opposing powers of the separate lens groups, chosen to flatten the field of view or to provide a zoom focal length change, consort with each other to scale up the effect. It is not uncommon for this longitudinal error to reach 1/500 or even 1/200 of the focal length [3].

Secondary spectrum effects also show themselves as a similar but transverse effect off axis, but in this case systems which are symmetrical about the aperture stop are automatically corrected for this error. In several classes of optical system however, such symmetry cannot be implemented (e.g. in eyepieces, telecentric profile projection lenses and many zoom optical systems), and transverse secondary spectrum effects can sometimes dominate the oblique aberration residuals.

Secondary spectrum is not all bad. Because of its problematic nature and because we often only need to design achromatic systems with simple glasses, the magnitude of the secondary spectrum serves as a useful guide to the allowable magnitide of other residual aberrations. The point here is that it is the lens designer's religious duty to make a lens design as good as it can straight-forwardly be made before anyone embarks on the expensive, time consuming and irrevocable business of manufacture.

The secondary spectrum allows us to judge when we have done that job, so for example, Fig. 1 illustrates the familiar axial aberration curves for a typical achromatic system, where the red and blue aberration curves have been made to cross at the traditional 0.7 zonal aperture to within a small proportion of the secondary spectrum and the marginal spherical aberration has also been reduced to be a similarly small proportion of the secondary spectrum. Such practical secondary-spectrum-based tolerance rules apply for most of the other aberrations in highly corrected achromatic systems.

Notice that the dominant aberration in Fig. 1 is chromatic variation of spherical aberration between the red and the blue wavelengths.

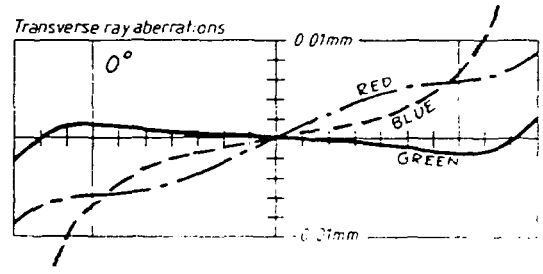

Fig.1 Typical axial aberration correction in achromatic optical systems f=100mm, f/5 (Thin doublet with K5 and F2 glass)

Catadioptric systems and the chromatic variation aberrations

If the focal power of an optical system is concentrated in reflecting surfaces and the correction of residual aberrations is allowed using refracting optical componets, it is possible to achieve high levels of performance over wider fields of view than is possible with purely reflecting systems [4]. Catadioptric optical systems, as one might expect, exhibit residual aberrations which are mostly composed of purely chromatic variation types.

Fig. 2 shows a straight forward example of this effect. The system illustrated in that diagram is the classic aspheric catadioptric Schmidt camera, whose

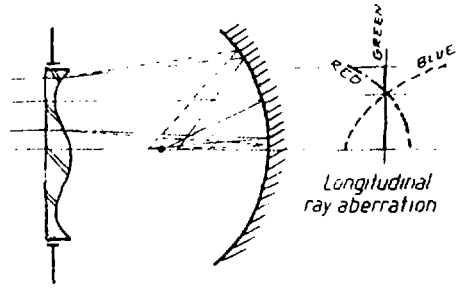

Fig.2 The chromatic variation of spherical aberration in the aspheric catadioptric Schmidt optical system.

residual aberrations on axis are an example of pure, unalloyed chromatic variation of spherical aberration without any secondary spectrum. This system also exhibits a chromatic variation of a higher order astigmatism off axis (an error which is higher order in aperture but not in field).

Fig. 3 shows a more illuminating case, where a reflecting Schwartzchild microscope objective has had a concentric hemispherical immersion component fitted at the microbe end (so to speak). The problem here arises

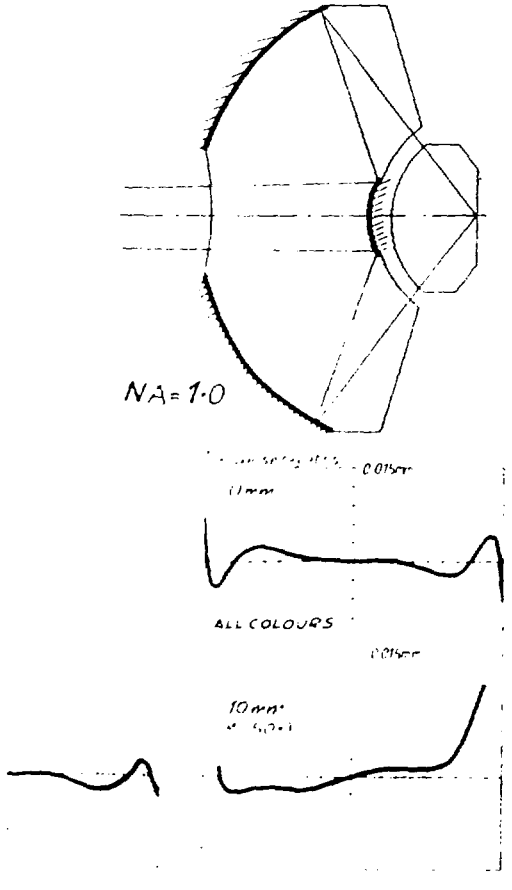

Fig.3 ASchwartzchild microscope objective with a concentric fluid immersion lens and zero working clearance.

not from the addition of the concentric immersion component, because, on axis at least, that component does not change the aberrations at all, but when the front working clearance is increased the refractive index and the dispersion difference between the immersion fluid and the front lens in that high numerical aperture space introduce spherical aberration and a chromatic variation of spherical aberration as shown in Fig. 4.

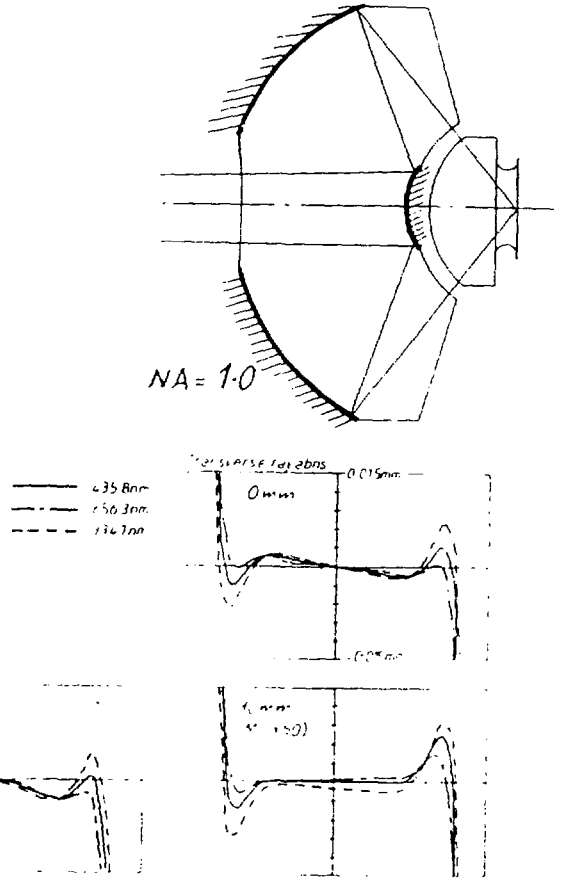

Fig.4 The same system as Fig. 3, but with the working clearance set at a finite value, showing spherical aberration and chromatic variation of spherical aberration.

The correction of the spherical aberration is a monochromatic affair and, at least in principle, it can be corrected with an adjustment to the mirror pair. The chromatic variation of the spherical aberration is however quite another matter because the mirror pair does not offer any chromatic aberration of any order or of either sign for the compensation of this error: from this simple logic we may conclude that the design must undergo a significant increase in chromatic aberration complexity if this error is to be corrected. That has indeed proved to be the case in this system, and although this problem has been solved (by the method

of managerial exhaustion referred to above) this case proved to me yet again how problematic chromatic variation aberrations can be. This is not a new problem and D.S.Grey has dealt at some length with the detailed solution methods in his classic paper [5] and its predecessors.

The general problem of chromatic variation aberrations

Although there are various tricks for the correction of chromatic variation aberrations which are known to practitioners in our trade they are usually only applicable in specific situations and there is no systematic methodology available to deal with the special problems that the correction of these aberrations present.

As an example of a specific well known trick, Fig. 5 shows the improvement that may be achieved in the aberrations of Fig. 1 if we exploit the separation of the red and blue rays that can be introduced in systems with finite thickness. Specifically, Fig. 5 shows the

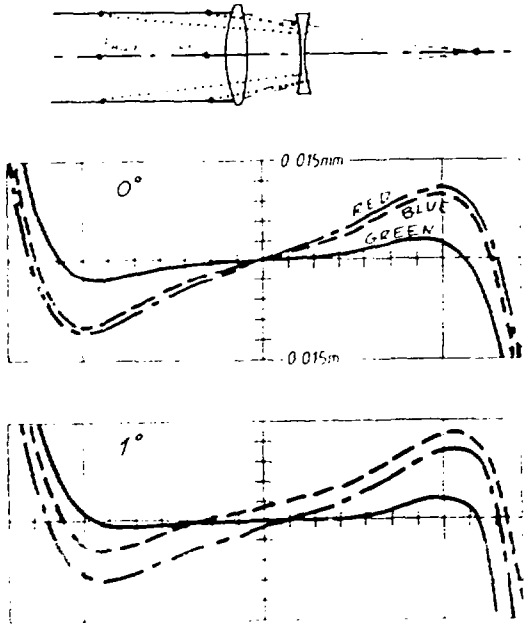

Fig.5 An airspaced achromatic doublet with correction for chromatic variation of spherical aberration f=100mm, f/5, K5 + F2

aberration curves for a simple achromatic doublet where the two components have been separated to allow the red and the blue rays of the axial pencil to separate at the second component, thereby reducing the overcorrection of the blue spherical aberration relative to the red. Although the spherochromatism has in this case been corrected, the zonal spherical aberration is worse and we have introduced transverse chromatic aberration.

In more complex systems we may anticipate the type of devices that may be helpful because if, as the last example suggests, it is the separation of the red and blue (or equivalent end-of-spectral-band) rays that is the critical mechanism, then we can use chromatically uncorrected components and spaces between components and surfaces in the system to achieve this requirement. Further, we may anticipate that highly dispersive materials in that context may be particularly useful, or even thin doublets with glass types specifically chosen to separate the "red" and "blue" rays, that is hyperchromatic combinations rather than chromatic combinations.

Again, this suggestion is not new [6]; but on the other hand there does not exist in the literature any systematic treatment of the methods whereby such devices may be applied.

Correction devices

In Fig. 6 I have illustrated the principle on which we may begin to think about the way such a method may be developed. A thin pair of plane parallel plates made of two materials with different dispersions, but having the same refractive index, make an obvious starting point for a chromatic ray separator which, at a naive level, does not have any monochromatic aberrations if it is in collimated space, whatever the curvature of the contact surface.

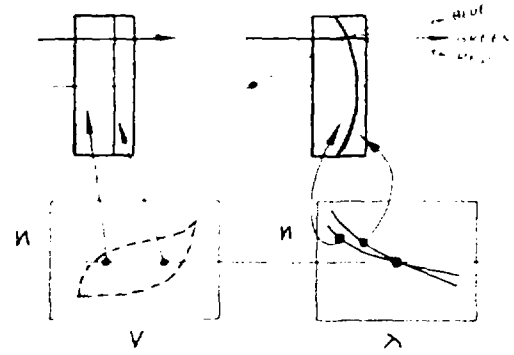

Fig.6 An initially "lazy" chromatic ray separation/combination doublet

Such a chromatic ray separator is a "lazy" component, in the sense that it does not help with the monochromatic aberration correction load. In a final

lens design for manufacture it would be usual to optimise the design, allowing the power, the shape and the index difference of the doublet to contribute to the available design variables.

For the chromatic variation aberration along any ray to be small at the final image it is necessary for the "red" and "blue" rays to arrive at the same point in the image; and this is not difficult to achieve for any one ray (for example, for the ray at the 0.7 zone of the aperture in the lens corresponding to the aberration curves in **Fig. 1**). The challenge is to achieve this for a wide range of rays, as has been done in the lens in **Fig. 5**, where at least on axis all the "red" and "blue" rays all arrive together. In the lens of **Fig. 5** we have transverse chromatic aberration and that corresponds to a variation of focal length with wavelength; and sure enough, we can see in **Fig. 5** that the principal point positions for the red and blue rays are at different positions. So, in general, we not only require the chromatic ray pair to arrive at the same image point, but to arrive at the same image point with the same directions.

Thus we see in **Fig. 7** that if all the chromatic ray separation management is to be done with initially-lazy, monochromatically inert doublets as described above we would need three of them in the system, the first one to separate the chromatic rays, the middle one to redirect them to be together at the third one and the third one to co-linearise the chromatic rays for their journey to the image. Additionally, the solution has to be such that this condition applies for all the rays of the pencil, so that when the field point changes there is no transverse separation of the chromatic rays for any of the aperture points. This is what I think could reasonbly be called chromatic isoplanatism.

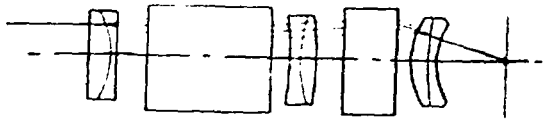

Fig.7 A complex starting system with three "lazy" concentric chromatic ray separation management doublets.

Chromatic isoplanatism in conventional systems

In conventional optical systems, which in this context means systems without initially-lazy chromatic rays separators/combiners, just such a mechanism is frequently evoked.

So, for example, in the classical Taylor-Cooke triplet, the ray at the 0.7 aperture zone on axis behaves in exactly this way, as shown in **Fig. 8**. However, this system is not generally corrected for chromatic variation aberrations because it is only that axial ray which is so perfectly corrected and we may expect that, off axis, such a system will suffer from chromatic variation of coma, corresponding to the chromatic variation of (spherical) aberration on axis, which in turn results from the lack of positional and angular coincidence of the red and blue rays.

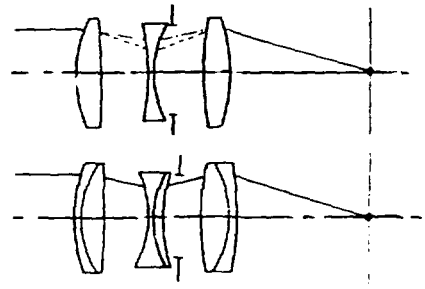

Fig.8 Chromatic ray separation in the Taylor-Cooke triplet and the three-achromat version of the same lens.

In principle one could devise initially-lazy "concentric" plates close to each lens of the triplet, each with an apherised ghost contact surface ($n_A - n_B = 0$) to correct the chromatic separation errors on axis. Such a concept is shown in **Fig. 9**. Also shown in **Fig. 9** is a more exotically impractical system with the aspheric contacts built into each of the three existing components! The ghost aspheric in each case needs to be normal to the already-corrected zonal ray.

This is not the way to design practical lens systems but the concepts do suggest methods of calculation for systems with chromatic variation aberration problems.

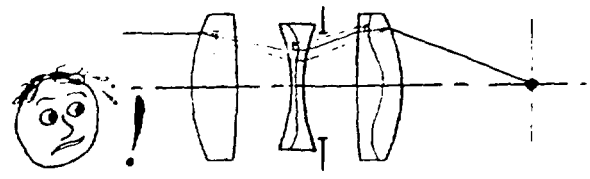

Fig.9 The deployment of chromatic ray separation management doublets with aspheric surfaces for a Taylor-Cooke triplet system.

WATER MOG, NA=1 OF MOPE FILE= :MAINT1: 10/4/94

FOCAL LENGTH= 3.8507

WAVELENGTH = .00040470 LAGRANGE INVARIANT = -.200000

H	U	A	D(U-N)	HBAR	UBAR	ABAR	E
2.524689	.020000	-.342583	.071351	-1.197438	.069732	.241702	2.371458
2.888121	.141652	.045146	.001471	-1.238738	-.016097	.049886	2.144540
3.392487	.142040	-.320471	-.061827	-1.294374	-.015668	.181227	1.907706
3.392642	.030995	.188110	-.053335	-1.294138	.047128	-.012804	1.907271
2.590369	-.034186	.815052	.740825	-.084020	.051565	.050772	.162178
22.750005	-1.099450	.241273	-1.230895	.187254	-.014794	.010777	-.041155
8.382510	-.784108	-.283620	-.369973	.174264	-.000709	.017963	-.103945
4.682142	-.882384	-.660565	.455328	.197393	.005515	.014867	-.210793
2.977823	-.653495	-1.000000	-.127541	.198342	.000364	.000557	-.333032
	-.744713				.000415		

S1	S2	S3	S4	S5	C1	C2
-.021142	.014916	-.010524	-.002040	.008864	-.026630	.018788
-.200009	-.000010	-.000011	.000013	.000003	-.001390	-.001536
.021541	-.012182	.006889	.001436	-.004709	.021886	-.012377
.006401	-.000436	.000030	.000642	-.000046	.012847	-.000874
-1.274620	-.079413	-.004947	.011440	.000404	0.000000	0.000000
1.630130	.072814	.003252	-.002164	.000049	0.000000	0.000000
.249470	-.015800	.001001	-.000990	-.000001	.047860	-.003031
-.430251	.020937	-.000471	.000657	-.000004	-.062262	.001401
.374795	-.000211	.000000	0.000000	-.000000	.010936	-.000006
.061114	.000615	-.004781	.003993	.004562	.003248	.002366

ALL THE FOLLOWING VALUES ARE DIFFERENCES EXCEPT U , UBAR

WAVELENGTH = .00050660 LAGRANGE INVARIANT = -.200000

H	U	A	D(U-N)	HBAR	UBAR	ABAR	E
-.000001	0.000000	-.000000	-.000456	.000001	-.000000	-.000000	-.000002
-.004917	-.001925	-.003053	-.000298	.003486	.001358	.001448	-.002369
-.012105	-.002018	.000802	.000303	.008056	.001289	-.000421	-.005096
-.012102	-.000452	-.001013	.000743	.008064	.000415	.000788	-.005093
.003214	.000653	-.002932	.005493	.010248	.000093	.003241	-.019957
.040987	-.002060	-.000920	-.009815	.094185	-.004578	.000966	-.020590
.016551	-.001333	.001508	.004361	.035181	-.003220	-.001186	-.020739
.017919	.000326	.001175	-.004756	.019670	-.003699	-.002767	-.020122
.010760	-.002738	.001964	-.000127	.012651	-.002691	-.004096	-.019964
	-.747033				-.002649		

S1	S2	S3	S4	S5	C1	C2
.000135	-.000095	.000067	.000032	-.000070	-.000232	.000164
.000003	.000002	.000002	-.000002	-.000001	.000079	-.000063
-.000289	.000161	-.000090	-.000017	.000059	.000001	-.000003
-.000179	.000036	-.000004	-.000007	.000003	-.000036	.000052
-.001810	-.005495	-.000700	.000071	-.000015	0.000000	0.000000
.000350	.006998	.000647	-.000013	.000036	0.000000	0.000000
-.000074	.001266	-.000136	.000012	.000007	.000134	.000177
.009484	-.004040	.000161	-.000008	-.000002	-.000512	-.000249
.000256	.001559	.000005	0.000000	.000000	.000138	.000045
.005876	.000393	-.000043	.000067	.000018	-.000428	.000122

Table 1 Seidel three-colour difference calculations.

Calculation methods for chromatic variation aberrations

(i) *Differential chromatic ray tracing:*
The most obvious artifice to come out of the type of thinking that I have applied above is to display the separate paths that the "red" and "blue" rays follow through the optical system. If one were to do that literally, the ray separations would certainly be lost beside the magnitude of the monochromatic ray heights,so that the natural way to implement the requirement is to display the differences in height at each optical surface relative to one of the two chromatic rays, or perhaps more practically, relative to the mean wavelength ray, so that we may also see the secondary spectrum. This is shown in **Fig. 10** for the case of a thin doublet and an equivalent airspaced doublet where the chromatic variation of spherical aberration has been corrected.

(ii) *Chromatic change in Seidel coefficients:*
Another obvious calculation method results from calculating Seidel coefficients along the different chromatic ray paths and then taking differences. This is not as elegant as deriving chromatic differential versions of the standard Seidel formulae as for example H.H.Hopkins has done [7], but it hasthe advantage of zero doubt about the results when large chromatic ray separations are involved, as they are when we are dealing with chromatic variation aberrations in widely spaced systems, such as those that are corrected for field curvature. **Table 1** shows typical output for such a calculation, where "red" and "blue" values have been differenced from the "green" values to reveal the chromatic differences.

(iii) *Chromatic variation of chromatic difference wavefront aberration computed using the Conrady formula.*
Finally, **Fig. 11** shows the result using the Conrady chromatic difference formula [8]

$$\delta W = \Sigma \delta n \, (D\text{-}\overline{D})$$

the first system shown in the diagram is a thin achromat where there is only small chromatic ray separation and, as might be expected the δW curve is very similar when computing along each of the three separate chromatic ray paths. The second system shown in **Fig. 11** is corrected for the chromatic variation of spherical aberration and this is also clear from the mean wavelength ray path Conrady wavefront difference plot. However, that plot is not to be trusted because when the same

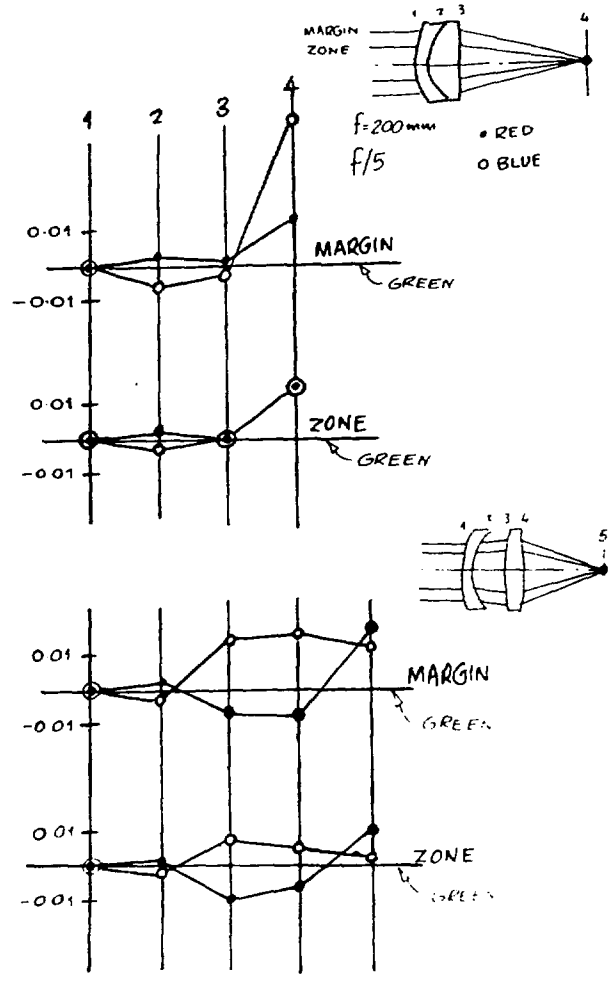

Fig. 10 Chromatic differential ray tracing in thin and thick systems.

error is calculated using the red and blue ray paths the results change, due to the finite ray separations. The variation between these three plots clearly contains useful information, which I have not yet exploited. The exploitation of this information will be the subject of a future paper, as they say.

Conclusions

- The chromatic variation of aberrations are an important barrier to the improvement of refracting and catadioptric optical systems.
- Contemporary lens design software does not cope well with the high gear ratio that exists between these errors and the constructional changes that are necessary to correct them.

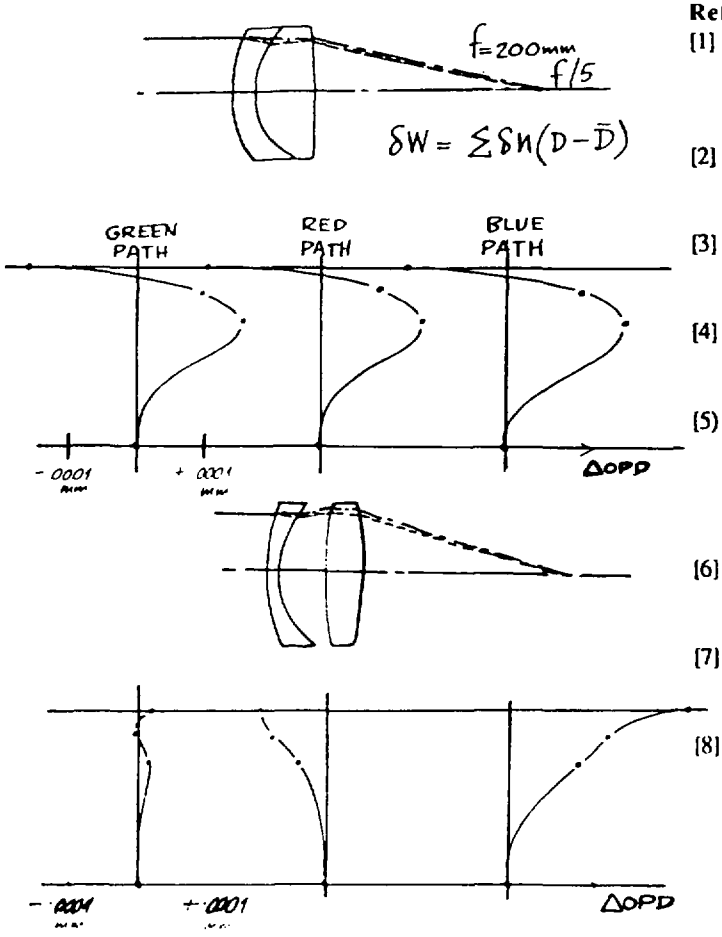

Fig.11 The use of Conrady D-D chromatic wavefront aberration calculations in thin and thick systems

We may understand the origin and the correction strategies that apply to these aberrations by studying the chromatic separation of rays, because if the different chromatic rays coincide in both position and direction at any point in the image for all aperture points then we have a condition which corresponds to a chromatic version of the isoplanatism condition (the sine condition).

There are several fairly obvious aberration calculation methods which may be applied to the chromatic variation aberrations, three of these have been reviewed.

References

[1] Sigler,R; *Glass selection for air spaced apochromats using the Buchdahl dispersion equation.* Appl. Opt. 25; p4311-4320 (1986)

[2] Kingslake,R; *Lens design fundamentals.* Academic Press, p133-136, 1978.

[3] Maxwell,J; *Tertiary spectrum manipulation in apochromats.* Appl. Opt. 31, p2194-2198 (1992)

[4] Maxwell,J; *Catadioptric Imaging Systems;* Hilger and Elsevier 1972.

[5] Grey,D.S; *A new series of microscope objectives:III ultraviolet objectives of intermediate numerical aperture.* J. Opt. Soc. Am.40, p283-290 (1950).

[6] Hovestadt,H; *Jena glass* (English translation) Macmillan, p37-39 and p108-110, 1902.

[7] Hopkins,H.H; *Wave theory of aberrations*: Oxford p80, 1950

[8] Conrady, A.E; *Article in the Dictionary of Applied Physics (Vol 4 p202-237) on the optics oft the microscope*, (Ed Sir Richard Glazebrook), Macmillan,1923.

Ghanaian Participants

Dr. Yaw Opoku-Ankomah
Water Resources Inst.,
(CSIR)
P. O. Box M. 32,
Accra.

Mr. John K Kutor,
Dept. of Physics,
University of Ghana,
Legon

Mr. Samuel D. Asiamah,
Dept. Of Physics,
University of Ghana,
Legon

Mr. Ishmael K. Anderson,
L6 Akuafo Hall,
University of Ghana,
Legon

Mr. Daniel Obuobi,
Computer Centre,
University of Cape Coast

Mr. Francis Baffoe-Ashun,
Scientific Instrumentation
Center (CSIR),
P.O.Box M.32
Accra

Dr. George E Armah,
Noguchi Memorial Institute
for Medical Research,
P.O.Box 25,
University of Ghana,
Legon.

Mr. L.A. Ahen
Dept. of Physics
University of Cape Coast

Mr. Godwin Quaye Okai,
Scientific Instrumentation
Centre (CSIR),
P.O.Box M.32
Accra

Mr. Charles E.Amoh
B.N.A.R.I.
Ghana Atomic Energy Commission,
P.O. Box 80,
Legon.

Mr. J.B. Gyamfin Owusu
Depart of Mathematics
U.S.T.
Kumasi

Mr. K.A. Otu-Danquah,
Ministry of Energy & Mines,
PMB, Ministries Post Office,
Accra

Mr. Joseph B. Awotwi-Pratt
Ministry of Energy & Mines,
PMB, Ministries Post Office,
Accra

Mr. Ben Appiah Agyare
Ministry of Energy & Mines,
PMB, Ministries Post Office,
Accra

Clement Entsua-Mensah
Ministry of Energy & Mines.
PMB, Ministries Post Office
Accra

Mr. Joseph Essandoh-Yeddu,
Ministry of Energy & Mines,
PMB, Ministries Post Office
Accra.

Mr. Eugen Adjei Johnson
Pysics Department,
University of Cape Coast

Mr. Asamoah Bosomtwi,
Physics Department,
University of Cape Coast

Mr. Moses Jojo Eghan,
Physics Department,
University of Cape Coast

Mr. Eric Ampem Lassen,
Physics Department
University of Cape Coast

Mr. M.K. Akyena,
P & T Corporation,
Headquarters
Accra North

Mr. Charles D. Tulashie,
Boa Amponsem Sec. School,
P.O. Box 225
Dunkwa-on-Offin

Mr. Alex Asante,
Computer Centre,
University of Cape Coast.

**Designed and Published by the Public Affairs Department,
Ghana National Petroleum Corporation.**